UNIVERSIDAD DE CONCEPCIÓN

Centro de Investigación en Ingeniería Matemática (CI^{2}MA)

A numerical scheme for a model of a flotation column including the transport of liquid components

Raimund Bürger, Stefan Diehl,
María Carmen Martí, Yolanda Vásquez

PREPRINT 2025-17

SERIE DE PRE-PUBLICACIONES

A NUMERICAL SCHEME FOR A MODEL OF A FLOTATION COLUMN INCLUDING THE TRANSPORT OF LIQUID COMPONENTS

RAIMUND BÜRGER[A], STEFAN DIEHL[B], MARÍA DEL CARMEN MARTÍ[C], AND YOLANDA VÁSQUEZ[D]

Abstract. Froth flotation in a column is a widely used unit operation in mineral processing, wastewater treatment, and other applications. The flotation process selectively separates finely divided hydrophobic materials (valuable minerals or ores; repelled by water) from hydrophilic (slimes or gangue; attracted to water), where both are suspended in a viscous fluid. A flotation column roughly functions as follows: gas is introduced close to the bottom and generates bubbles that rise through the continuously injected pulp that contains the solid particles. The hydrophobic particles attach to the bubbles, forming foam or froth (the concentrate) that is removed through a launder. The hydrophilic particles do not attach to bubbles, but normally settle to the bottom, and are removed continuously. Additional wash water, injected close to the top, may assist with the rejection of entrained impurities and increase froth stability. A recently formulated partial differential equation model [R. Bürger, S. Diehl, M.C. Martí, Y. Vásquez, *IMA J. Appl. Math.* **87** (2022) 1151–1190] describes the process by a pair of degenerate parabolic PDEs with discontinuous flux for the volume fractions of bubbles and hydrophilic solid particles as functions of height and time. An extension of that model is presented, which includes the effect of wash water to be injected into the froth as well as the transport of an arbitrary number of components (such as slimes or chemical reagents) with the liquid. The numerical scheme for bubble and particle volume fractions is extended to simulate percentages representing the liquid components, which are proven to remain nonnegative and sum up to one. In addition, a theory of desired steady states of the flotation column is outlined. It is proven that the condition of "positive bias" in a determined zone of the flotation column (i.e., net downward flow of water) coincides with the mathematically derived condition for the existence of a stationary bubble concentration profile, including a stable froth layer. It is demonstrated how steady-state solutions to the governing model can be constructed and conditions for their existence can be conveniently mapped through so-called "operating charts." Numerical simulations are presented.

1. Introduction

1.1. **Scope.** Froth flotation in a column is a unit operation widely used in mineral processing and wastewater treatment. In the latter application, flotation is a pre-treatment for reducing oil droplets and fat. In the former application it serves to separate valuable mineral particles from worthless gangue particles in finely ground ores. The valuable mineral particles are hydrophobic

Date: September 8, 2025.

Key words and phrases. Flotation column; three-phase flow; component transport; degenerate parabolic equation; monotone scheme; steady state; operating chart; bias flow.

*Corresponding author.

[A]CI^{2}MA and Departamento de Ingeniería Matemática, Facultad de Ciencias Físicas y Matemáticas, Universidad de Concepción, Casilla 160-C, Concepción, Chile. E-Mail: rburger@ing-mat.udec.cl.

[B]Centre for Mathematical Sciences, Lund University, P.O. Box 118, S-221 00 Lund, Sweden. E-Mail: stefan.diehl@math.lth.se.

[C]Departament de Matemàtiques, Universitat de València, Avda. Vicent Andrés Estellés s/n, E-46100 Burjassot, València, Spain. E-Mail: Maria.C.Marti@uv.es.

[D]Facultad de Ciencias y Tecnología, Universidad Tecnológica de Panamá, Panama. E-Mail: yolanda.vasquez@utp.ac.pa.

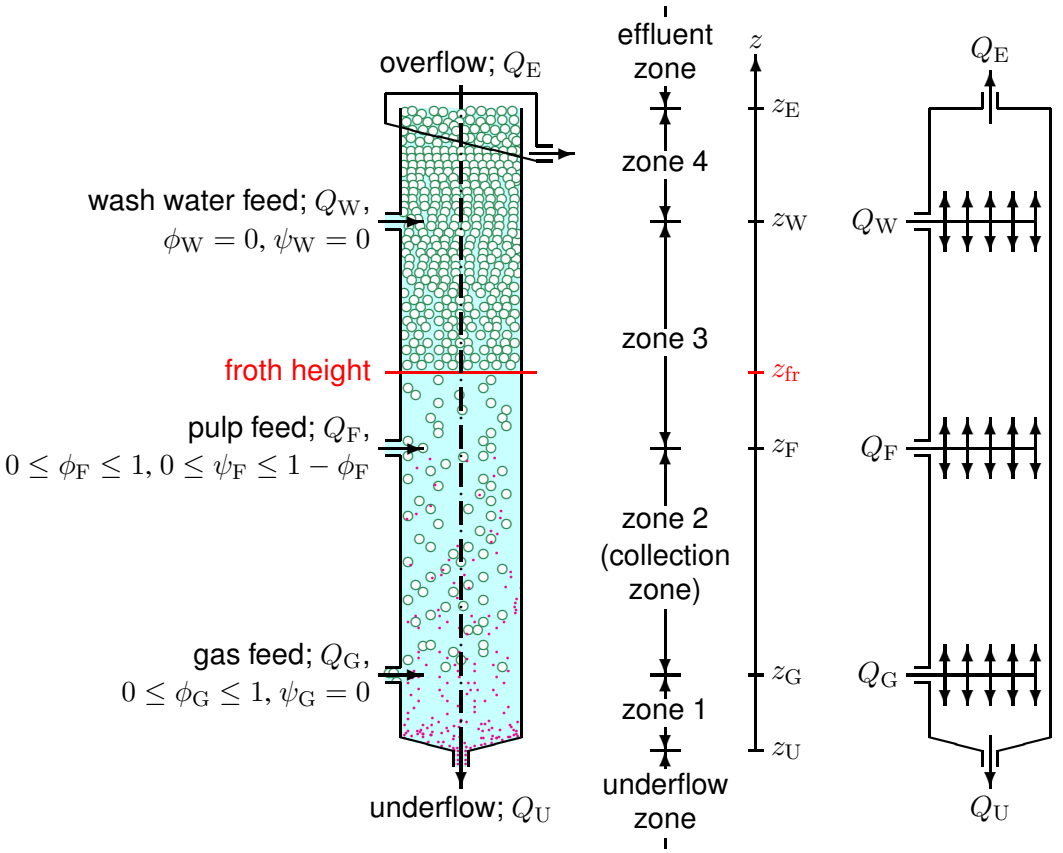

FIGURE 1. Schematic of a froth flotation column: (left) denomination of zones, (middle) height axis (z-axis) showing the location of feed and discharge levels, (right) schematic of the column. The open circles and solid magenta dots represent bubbles and hydrophilic particles, respectively. The information to the left indicates the overflow or effluent rate Q_{E}, volume feed rates (Q_{W}, Q_{F}, and Q_{G}) and concentrations (ϕ_{W}, ψ_{W}, ϕ_{F}, ψ_{F}, ϕ_{G}, and ψ_{G}), and the underflow volume rate Q_{U}, along with limitations the feed concentrations must satisfy. The denomination of zone 2 as "collection zone" is common in mineral processing, although the process of collection (adhesion of hydrophobic particles to bubbles) is not part of the model.

and attach to bubbles of air injected into the pulp. The bubble-particle aggregates rise to the top of the flotation column where they accumulate to a froth that is removed through a launder for further processing. At the same time, the hydrophilic gangue particles settle and are removed continuously (see Figure 1). The drainage of liquid due to capillarity is essential for the formation of stable froth. A small amount of water, the so-called "wash water," is sprinkled onto the top of or is injected into the froth. The introduction of wash water assists with the rejection of entrained impurities (slimes), tends to increase froth stability, and contributes to better recovery [23, 25, 30, 33]. A part of the wash water overflows with the froth bubbles and the remaining part flows down the froth counter-current to the gas phase and is referred to as bias water. In the engineering literature (see, e.g., [6, 12, 21, 23]) a net downward flow of water through the froth is usually referred to as "positive bias," see Figure 2.

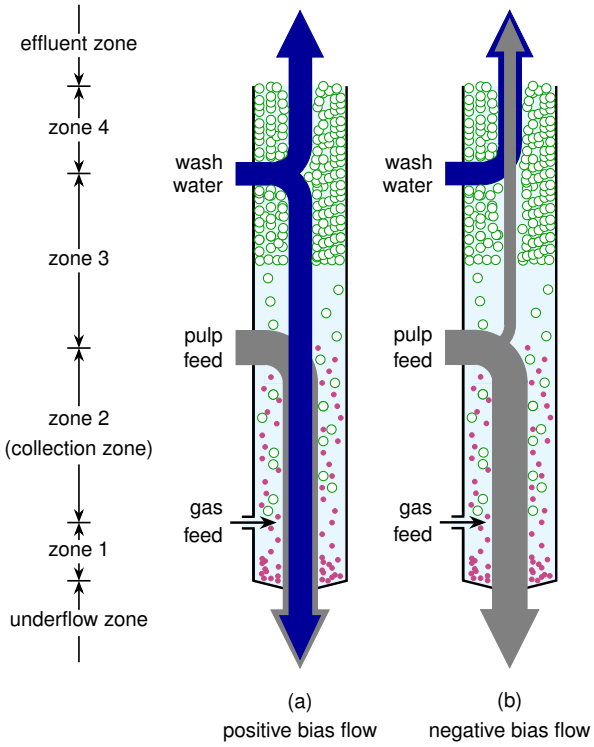

FIGURE 2. Schematic of the concepts of (a) "positive bias" and (b) "negative bias" in a froth flotation column (after [21, Fig. 8]), which refers to wash water passing zone three downwards.

A three-phase model describing the stationary and transient behaviour of a flotation column with drainage for a one-dimensional setup (slightly different from that of Figure 1) was developed in [10]. For the column drawn in Figure 1 this model can be written as the system of partial differential equations (PDEs)

$$\begin{aligned} &A(z)\partial_t \begin{pmatrix} \phi \\ \psi \end{pmatrix} + \partial_z \left(A(z) \begin{pmatrix} J(\phi,z,t) \\ -\tilde{F}(\psi,\phi,z,t) \end{pmatrix} \right) \\ &= \partial_z \left(A(z)\gamma(z) \begin{pmatrix} 1 \\ -\psi/(1-\phi) \end{pmatrix} \partial_z D(\phi) \right) + \sum_{S\in\{\mathrm{G,F,W}\}} Q_S(t) \begin{pmatrix} \phi_S(t) \\ \psi_S(t) \end{pmatrix} \delta(z-z_S), \end{aligned} \tag{1.1}$$

where $z \in \mathbb{R}$ is height, $t > 0$ is time, $A(z)$ is the cross-sectional area of the column at height z, $\phi = \phi(z,t)$ is the volume fraction of bubbles, $\psi = \psi(z,t)$ is the volume fraction of gangue (hydrophilic) solid particles, $J = J(\phi,z,t)$ and $\tilde{F} = \tilde{F}(\psi,\phi,z,t)$ are convective flux functions that depend discontinuously on z at the locations of the gas inlet ($z = z_\mathrm{G}$), the pulp feed inlet ($z = z_\mathrm{F}$), the wash water inlet ($z = z_\mathrm{W}$), the underflow outlet ($z = z_\mathrm{U}$) at the bottom, and the overflow outlet ($z = z_\mathrm{E}$) at the top, see Figure 1. The characteristic function γ indicates the interior of the column:

$$\gamma(z) := \begin{cases} 1 & \text{inside the column, i.e., if } z_\mathrm{U} \le z \le z_\mathrm{E}, \\ 0 & \text{outside the column, i.e., if } z < z_\mathrm{U} \text{ or } z > z_\mathrm{E}. \end{cases}$$

The function D models the capillarity, which is in effect when the bubbles are in contact. This is assumed to occur whenever $\phi > \phi_\mathrm{c}$, where ϕ_c is a given critical bubble volume fraction that marks

the interface between pulp (where $\phi \le \phi_c$) and froth (where $\phi > \phi_c$). The function D is given by

$$D(\phi) := \int_0^\phi d(s)\,\mathrm{d}s, \quad \text{where} \quad d(\phi) = D'(\phi) \begin{cases} = 0 & \text{for } 0 \le \phi \le \phi_c, \\ > 0 & \text{for } \phi_c < \phi \le 1. \end{cases} \tag{1.2}$$

(Precise definitions of the underlying ingredients will be provided in Section 2.)

It is the purpose of this contribution, firstly, to extend the model (1.1) beyond the framework of [10] by the assumption that the liquid phase is subdivided into a number k_f of components. These components can be finely divided solids, so-called slimes; chemical substances such as reagents (chemicals added to enhance the flotation process, for instance collectors to make the mineral particles hydrophobic or frothers to help create a stable foam); or one may wish to mark portions of the fluid that enter through either the feed or the wash water inlet. These components give rise to a vector of percentages $\boldsymbol{p}$ for the components of the fluid phase. The final partial differential equation governing the evolution of $\boldsymbol{p} = \boldsymbol{p}(z,t)$ is given by

$$\begin{aligned} &\partial_t(A(z)\phi_f \boldsymbol{p}) + \partial_z\left(A(z)\left(q - J(\phi,z,t) + \tilde{F}(\psi,\phi,z,t) + \gamma(z)\frac{1-\phi-\psi}{1-\phi}\partial_z D(\phi)\right)\boldsymbol{p}\right) \\ &= Q_F(t)\phi_{f,F}(t)\boldsymbol{p}_F(t)\delta(z-z_F) + Q_W(t)\phi_{f,W}(t)\boldsymbol{p}_W(t)\delta(z-z_W), \end{aligned} \tag{1.3}$$

where $\phi_{f,F}(t)$ is the fluid volume fraction and $\boldsymbol{p}_F(t)$ the percentage vector associated with the pulp feed, and $\phi_{f,W}(t)$ and $\boldsymbol{p}_W(t)$ are the corresponding quantities for the wash water. Notice that for given functions $\phi = \phi(z,t)$ and $\psi = \psi(z,t)$, suitable initial conditions and feed functions $\boldsymbol{p}_F(t)$ and $\boldsymbol{p}_W(t)$, (1.3) is a linear transport equation for $\boldsymbol{p} = \boldsymbol{p}(z,t)$ with singular source terms. It is demonstrated that the monotone numerical scheme introduced in [10], which can easily be adapted to handle (1.1), can be extended by a scheme to solve (1.3), and thereby to simulate the transport of these components or equivalently, the propagation of the percentage vector $\boldsymbol{p}$. The scheme approximating (1.3) is designed in such a way that under a suitable Courant–Friedrichs–Lewy (CFL) condition, the percentages are bounded between zero and one and sum up to one when the initial data have this property.

Secondly, we formulate a theory of stationary (steady-state) solutions of (1.1) that is based on the solution of suitable ordinary differential equations (ODEs) arising from (1.1) in the stationary case in combination with jump and entropy jump conditions, and which incorporates the effect of wash water. In particular, the condition of "positive bias" is cast in mathematical terms and leads to the concept of "desirable steady states."

Thirdly, we illustrate the new scheme by numerical examples that illustrate that the system attains, abandons, or recovers desirable steady states as predicted by the theory, and utilize the description of liquid components to provide numerical simulations that distinguish between water that initially fills the column, slimes (fine suspended particles that follow the fluid), and the two inflows of feed water and wash water. In particular situations of positive bias flow are simulated.

1.2. **Related work.** The present contribution is part of current efforts to design methods for multicomponent or multispecies transport, and flow problems in general, that would satisfy an "invariant region preservation (IRP)" principle. In the present context the IRP principle requires that the (numerically simulated) volume fractions ϕ and ψ should be nonnegative and sum up at most to one; and the percentages of components for the solid or liquid phase should be nonnegative and sum up to exactly one. Numerical schemes for conservation laws that would preserve the IRP or related properties were recently reviewed in [28]. On the other hand, the idea to augment an existing scheme for a scalar conservation law with discontinuous flux by a procedure to compute the transport of components was introduced in [13]. This approach was extended in [8] to models of

reactive settling including the transport of solid and liquid components. Related work on positivity- and bound-preserving schemes (i.e., that are endowed with an IRP property) includes [2,4,26,27]. Our approach leads to a scheme that is formally first-order accurate in space and time due to the first-order time discretization and usage of a monotone numerical flux. A related problem, namely convergence of entropy stable schemes for a degenerate parabolic equation (such as the ϕ-equation of (1.1)) with a discontinuous flux function, is studied in [1]. The concept of operating charts for the visualization of necessary inequalities for obtaining a steady-state solution was introduced in [14] to categorize steady-state solutions of the similar continuous-sedimentation process for the separation of biomass from liquid in wastewater treatment plants and utilized for control of steady states [15,16] and dynamic behaviour [17,18]. In [5], the use of operating charts for a flotation setup was in agreement with laboratory tests.

With respect to related work from the engineering literature, besides the references [6,12,25,30,32,33] cited within the model development elsewhere in this work, we mention handbooks or reviews related to the fundamentals of flotation columns in mineral processing (such as [21,23,24,31]) and wastewater treatment [20,29]. Other references can be found in [10].

1.3. **Outline of the paper.** The remainder of the paper is organized as follows. In Section 2, the three-phase model for a flotation column is deduced. Supposing that mass is conserved inside the column, we obtain in Section 2.1 a system of three balance equations for the time and spatial evolution of the volume fraction of three phases, namely aggregates (bubbles fully loaded with hydrophobic particles), hydrophilic solid particles and fluid, including three feed inlets in the column and the effect of the drainage of water that may occur at the top of the column when a froth layer is created. In Section 2.2 we incorporate the drift-flux and solid-flux theories that define the nonlinear dependence of J on ϕ and of $\tilde{F}$ on ϕ and ψ, respectively. The function $d(\phi)$ defining the capillarity term $D(\phi)$ in (1.2) is specified in Section 2.3. The new model ingredient, namely the system of PDEs (1.3) that governs the evolution of the vector of percentages $\boldsymbol{p} = \boldsymbol{p}(z,t)$, is derived in Section 2.4. Although the model handles an arbitrary number k_{f} of liquid components, we limit the numerical experimentation to the particular case $k_{\mathrm{f}} = 4$ addressed at the end of Section 1.1. The corresponding components and percentages are properly introduced in Section 2.5. In Section 3, we introduce the numerical scheme used for the simulation of the flotation process starting, in Section 3.1, with the discretization of (1.1) by a variant of the scheme introduced in [10] (in that work, for a different arrangement of feed and discharge openings). We outline the proof of monotonicity of the resulting scheme and demostrate that for suitable initial conditions, the numerical solution always satisfies $0 \le \phi \le 1$ and $0 \le \psi \le 1 - \phi$ in the appropriate discrete sense. Then, in Section 3.2, we add the discretization of (1.3) and prove its properties. Section 4 is devoted to the study of the steady-state solutions of the system satisfying that a froth layer appears at the top of the column, with no aggregates leaving at the underflow, and that there is a positive bias flow, i.e., there is a downwards directed water flow under the wash water inlet, which is crucial in real applications to clean the foam from entrained hydrophilic solid particles. These properties, listed in Section 4.1, are motivated by the conditions under which a flotation column should operate in engineering applications without the necessity to permanently apply control actions. We derive the necessary conditions for the so-called desired steady states to be feasible, in terms of inequalities involving the bulk velocities in each zone of the column, defined by the volumetric flows Q_{U}, Q_{G}, Q_{F} and Q_{W}, and the incoming volume fractions of aggregates ϕ_{G} and solids ψ_{F}. Next, in Section 4.2, we utilize the jump and entropy conditions [19] for a stationary solution of the degenerate parabolic equation with discontinuous flux function given by the ϕ-component of (1.1) (known from [5,10] for similar models of froth flotation) to construct a desirable steady-state solution for the aggregates. This

construction is feasible only if the operating parameters satisfy a total number of seven restrictions (conditions). A similar analysis is done in Section 4.3 for the solid particles, which yields three additional conditions. The total number of ten inequality conditions can be conveniently visualized in an operating chart, that is, by intersection of subregions in a q_{G} versus q_{U} plane, as is explained in Section 4.4. The theoretical results of Sections 3 and 4 are exemplified in Section 5 by a series of numerical examples. We show some simulations using the operating charts created from conditions in Section 4 to illustrate the dynamics of the column until it reaches a desired steady state. We also show some simulations to illustrate the response of the system to changes in the operating conditions. Finally, some conclusions and future work are presented in Section 6.

2. Governing model

2.1. **Phases, bulk flows and mass conservation.** The governing three-phase model is formed by two disperse phases, gas bubbles fully loaded with hydrophobic particles, referred to as the aggregates, and (hydrophilic) solid particles. Both are dispersed within the fluid, which is the third phase. The dimensionless volume fractions $\phi := \phi(z,t)$ of aggregates, $\psi := \psi(z,t)$ of (hydrophilic) solid particles and $\phi_{\mathrm{f}} := \phi_{\mathrm{f}}(z,t)$ of the fluid satisfy

$$\phi_{\mathrm{f}} + \psi + \phi = 1, \quad 0 \le \phi_{\mathrm{f}}, \psi, \phi \le 1. \tag{2.1}$$

We suppose that the column initially is filled with fluid. A height $z = z_{\mathrm{G}}$, only gas bubbles enter the column at a volumetric rate $Q_{\mathrm{G}} > 0$. Thus, the solid and liquid feed concentration at z_{G} are zero ($\psi_{\mathrm{G}}, \phi_{\mathrm{f,G}} \equiv 0$) while the feed bubble volume fraction at z_{G} is $\phi_{\mathrm{G}} = 1$. The process of adhesion of hydrophobic particles to bubbles is not included in the model, and is assumed to occur before the slurry enters the column so that the gas bubbles injected into the column are fully loaded with hydrophobic particles.

A mixture of slurry and water is fed at height $z = z_{\mathrm{F}}$ at the volumetric flow $Q_{\mathrm{F}} > 0$, with $\phi_{\mathrm{F}} \equiv 0$ and $\psi_{\mathrm{F}}, \phi_{\mathrm{f,F}} \in (0,1)$. Wash water is injected near the top of the column at height $z = z_{\mathrm{W}}$ at the volumetric flow $Q_{\mathrm{W}} > 0$. Only clear wash water is injected, which means $\phi_{\mathrm{W}} \equiv 0$, $\psi_{\mathrm{W}} \equiv 0$, and $\phi_{\mathrm{f,W}} \equiv 1$. All phases can leave the column through the underflow, at the bottom of the column at height $z = z_{\mathrm{U}}$, with volumetric flow $Q_{\mathrm{U}} > 0$, or through the effluent, located at the top of the column at height $z = z_{\mathrm{E}}$, with volumetric flow

$$Q_{\mathrm{E}} = -Q_{\mathrm{U}} + Q_{\mathrm{G}} + Q_{\mathrm{F}} + Q_{\mathrm{W}} > 0.$$

This assumption ensures that the mixture is conserved and the column is always completely filled.

The flotation column can be divided into zones, depending on the position of the inlets considered. The interior of the flotation column is divided into four zones; see Figure 1. We denote ‘ the subinterval $[z_{\mathrm{U}}, z_{\mathrm{G}})$ as ‘zone 1,” $[z_{\mathrm{G}}, z_{\mathrm{F}})$ as “zone 2,” $[z_{\mathrm{F}}, z_{\mathrm{W}})$ as “zone 3,” and $[z_{\mathrm{W}}, z_{\mathrm{E}})$ as “zone 4.” Moreover, we consider the “effluent zone,” where $z \ge z_{\mathrm{E}}$, and the “underflow zone,” where $z < z_{\mathrm{U}}$, outside the column.

The column may have a variable cross-sectional area with depth given by the function $A(z)$. For simplicity, we will consider a constant cross-sectional area above the gas inlet ($z \ge z_{\mathrm{G}}$) and let it be decreasing with depth in zone 1.

The conservation of mass for each of the three phases defines the system

$$\begin{aligned}
\partial_t(A(z)\phi) + \partial_z(A(z)\phi v_{\mathrm{a}}) &= Q_{\mathrm{G}}(t)\phi_{\mathrm{G}}(t)\delta(z - z_{\mathrm{G}}),\\
\partial_t(A(z)\psi) + \partial_z(A(z)\psi v_{\mathrm{s}}) &= Q_{\mathrm{F}}(t)\psi_{\mathrm{F}}(t)\delta(z - z_{\mathrm{F}}),\\
\partial_t(A(z)\phi_{\mathrm{f}}) + \partial_z(A(z)\phi_{\mathrm{f}} v_{\mathrm{f}}) &= Q_{\mathrm{F}}(t)\phi_{\mathrm{f,F}}(t)\delta(z - z_{\mathrm{F}}) + Q_{\mathrm{W}}(t)\phi_{\mathrm{f,W}}(t)\delta(z - z_{\mathrm{W}})
\end{aligned} \tag{2.2}$$

of balance equations for the time and spatial evolution of the volume fractions, where v_{a}, v_{s} and v_{f} are the phase velocities of the aggregates, solid and fluid, respectively. The right-hand sides describe the three singular sources z_{G}, z_{F}, and z_{W}, with $Q_S(t)$, $S \in \{\mathrm{G}, \mathrm{F}, \mathrm{W}\}$, the corresponding volume feed rate and $\phi_S(t)$, $\psi_S(t)$, and $\phi_{\mathrm{f},S}(t)$ the aggregates, solids and fluid volume fraction at each feed inlet, respectively. (This notation is consistent with [10].)

We define the volume-average velocity, or bulk velocity, of the mixture as

$$q \coloneqq \phi v_{\mathrm{a}} + \psi v_{\mathrm{s}} + \phi_{\mathrm{f}} v_{\mathrm{f}}. \tag{2.3}$$

Adding up the three equations in (2.2) and considering that $A(z)q(z,t) = -Q_{\mathrm{U}}(t)$ for $z < z_{\mathrm{G}}$ yields

$$q(z,t) \coloneqq \begin{cases} q_4 = q_{\mathrm{E}} \coloneqq (-Q_{\mathrm{U}} + Q_{\mathrm{G}} + Q_{\mathrm{F}} + Q_{\mathrm{W}})/A & \text{in zone 4 and the effluent,} \\ q_3 \coloneqq (-Q_{\mathrm{U}} + Q_{\mathrm{G}} + Q_{\mathrm{F}})/A & \text{in zone 3,} \\ q_2 \coloneqq (-Q_{\mathrm{U}} + Q_{\mathrm{G}})/A & \text{in zone 2,} \\ q_1 = q_{\mathrm{U}} \coloneqq -Q_{\mathrm{U}}/A & \text{in zone 1 and the underflow.} \end{cases}$$

2.2. **Drift-flux and hindered-settling functions.** The functions $J(\phi, z, t)$ and $\tilde{F}(\psi, \phi, z, t)$ in (1.1) are defined based on the constitutive functions for the aggregates batch flux $j_{\mathrm{b}}(\phi)$ and the solid batch sedimentation flux $f_{\mathrm{b}}(\varphi)$, respectively, where φ denotes the volume fraction of solids within the suspension that fills the interstices between bubbles:

$$\varphi \coloneqq \frac{\psi}{\psi + \phi_{\mathrm{f}}} = \frac{\psi}{1 - \phi}.$$

Following [9], we define the total convective fluxes for ϕ and φ as:

$$J(\phi, z, t) = \begin{cases} j_{\mathrm{E}}(\phi, t) \coloneqq q_{\mathrm{E}}(t)\phi & \text{in the effluent zone,} \\ j_k(\phi, t) \coloneqq q_k(t)\phi + j_{\mathrm{b}}(\phi) & \text{in zone } k = 1, \dots, 4, \\ j_{\mathrm{U}}(\phi, t) \coloneqq q_1(t)\phi & \text{in the underflow zone,} \end{cases} \tag{2.4}$$

$$F(\varphi, \phi, z, t) = \begin{cases} f_{\mathrm{E}}(\varphi, \phi, t) \coloneqq -(1-\phi) q_{\mathrm{E}}(t)\varphi & \text{in the effluent zone,} \\ f_k(\varphi, \phi, t) \coloneqq (1-\phi) f_{\mathrm{b}}(\varphi) + \big(j_k(\phi, t) - q_k(t)\big)\varphi, & \text{in zone } k = 1, \dots, 4, \\ f_{\mathrm{U}}(\varphi, \phi, t) \coloneqq -(1-\phi) q_1(t)\varphi & \text{in the underflow zone.} \end{cases} \tag{2.5}$$

The functions $f_k(\varphi, \phi, t)$ are positive in the direction of sedimentation, that is, decreasing z, while the functions $j_k(\phi, t)$ are positive in an increasing z direction. Figure 3 shows graphs of the zone flux functions $j_k(\phi)$ in (2.4).

From (2.5), we define the convective flux for the solids in (1.1) by

$$\tilde{F}(\psi, \phi, z, t) \coloneqq \begin{cases} F\big(\psi/(1-\phi), \phi, z, t\big) & \text{if } 0 \le \phi < 1, \\ 0 & \text{if } \phi = 1. \end{cases}$$

The constitutive functions for $j_{\mathrm{b}}(\phi)$ and $f_{\mathrm{b}}(\varphi)$ arising in (2.4) and (2.5), are given by $j_{\mathrm{b}}(\phi) \coloneqq \phi\tilde{v}(\phi)$ and $f_{\mathrm{b}}(\varphi) \coloneqq \varphi v_{\mathrm{hs}}(\varphi)$, where $\tilde{v}(\phi)$ is a given drift-flux velocity function and $v_{\mathrm{hs}}(\varphi)$ is a given hindered-settling function. We herein adopt the common Richardson–Zaki expression [32]

$$v_{\mathrm{hs}}(\varphi) = v_\infty (1 - \varphi)^{n_{\mathrm{RZ}}}, \tag{2.6}$$

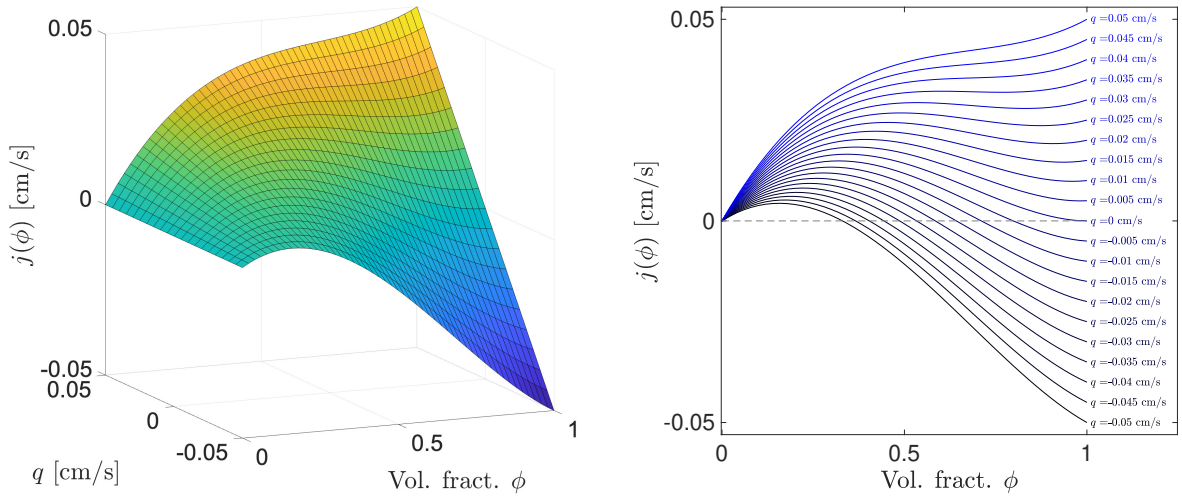

FIGURE 3. Graphs of zone flux functions $j(\cdot; q)$ for different bulk velocities q.

where v_∞ is the velocity of a single particle and n_{RZ} is a parameter satisfying $n_{\mathrm{RZ}} > 1$. On the other hand, as in [10] we define

$$\tilde{v}(\phi) := \begin{cases} v_{\mathrm{term}}(1-\phi)^{n_{\mathrm{b}}} & \text{for } 0 \le \phi \le \phi_{\mathrm{c}}, \\ v_{\mathrm{term}} \dfrac{(1-\phi)^{2n_{\mathrm{S}}+1}}{(1-\phi_{\mathrm{c}})^{2n_{\mathrm{S}}+1-n_{\mathrm{b}}}} & \text{for } \phi_{\mathrm{c}} < \phi \le 1, \end{cases} \tag{2.7}$$

where ϕ_{c} is the so-called critical concentration (see Section 1.1). A single bubble distant from others travels upward with the constant velocity $v_{\mathrm{term}} > 0$ (hence, $\tilde{v}(\phi) \ge 0$). The parameter n_{b} is a dimensionless constant. For $\phi > \phi_{\mathrm{c}}$, the liquid between the aggregates drains as they accumulate, creating a dry foam region at the top of the column. In [10], the second expression in (2.7) was derived for this scenario in detail, where n_{S} is a dimensionless constant.

2.3. **Capillarity.** When aggregates are in contact and foam is starting to form, it is necessary to take into account the effect of capillarity, i.e., the movement of the liquid through the narrow space between two adjacent bubbles as it drains from the foam layer. This drainage process results in the second-order spatial derivative terms in the PDE system (1.1) [10]. The generalized drainage equation expressed in ϕ is given by the function $\tilde{v}(\phi)$ in (2.7) and the function $d(\phi)$ defined by

$$d(\phi) := \begin{cases} 0 & \text{for } 0 \le \phi \le \phi_{\mathrm{c}}, \\ v_{\mathrm{term}} d_{\mathrm{cap}} \dfrac{\phi(1-\phi)^{n_{\mathrm{S}}}}{(1-\phi_{\mathrm{c}})^{2n_{\mathrm{S}}+1-n_{\mathrm{b}}}} & \text{for } \phi_{\mathrm{c}} < \phi \le 1, \end{cases} \tag{2.8}$$

with d_{cap} a capillarity-to-gravity constant present in the froth when $\phi > \phi_{\mathrm{c}}$; see [10] for a detailed deduction of this expression. From (1.2) and (2.8) we obtain

$$D(\phi) = \begin{cases} 0 & \text{for } 0 \le \phi \le \phi_{\mathrm{c}}, \\ v_{\mathrm{term}} d_{\mathrm{cap}} \dfrac{\omega(\phi_{\mathrm{c}}) - \omega(\phi)}{(1-\phi_{\mathrm{c}})^{2n_{\mathrm{S}}+1-n_{\mathrm{b}}}(n_{\mathrm{S}}+1)(n_{\mathrm{S}}+2)} & \text{for } \phi_{\mathrm{c}} < \phi \le 1, \end{cases} \tag{2.9}$$

where $\omega(\phi) := (1-\phi)^{n_{\mathrm{S}}+1}((n_{\mathrm{S}}+1)\phi + 1)$.

TABLE 1. Fixed values of some parameters.

Symbol	Significance	Value
z_{U}	underflow level	$0\,\mathrm{m}$
z_{G}	gas feed level	$0.07\,\mathrm{m}$
z_{F}	pulp feed level	$2.20\,\mathrm{m}$
z_{W}	wash water feed level	$2.70\,\mathrm{m}$
A	interior cross-sectional area	$0.018241\,\mathrm{m}^2$
v_∞	velocity of a single solid particle	$0.005\,\mathrm{m/s}$
n_{RZ}	dimensionless parameter in (2.6)	1.5
v_{term}	velocity of a single aggregate	$0.1\,\mathrm{m/s}$
n_{b}	dimensionless parameter in (2.7)	2
n_{S}	dimensionless parameter in (2.7)	0.46
d_{cap}	dimensionless capillarity-to-gravity constant in (2.9)	0.003331
ϕ_{c}	critical volume fraction of aggregates	0.74

The model development outlined so far specifies all ingredients of the governing system of equations (1.1). Some of the parameters have fixed values throughout this work, which are used to produce all figures, see Table 1.

2.4. **Components of the liquid phase.** By analogy with treatments of reactive settling [7, 8], we denote the total number of fluid components by k_{f}. The volume fractions of these components are $\phi_{\mathrm{f}}^{(l)} = \phi_{\mathrm{f}}^{(l)}(z,t)$, $l = 1,\dots,k_{\mathrm{f}}$, where we assume that

$$\begin{aligned} &0 \le \phi_{\mathrm{f}}^{(l)}(z,t) \le \phi_{\mathrm{f}}(z,t) \quad \text{for all } l = 1,\dots,k_{\mathrm{f}};\\ &\phi_{\mathrm{f}}^{(1)}(z,t) + \ldots + \phi_{\mathrm{f}}^{(k_{\mathrm{f}})}(z,t) = \phi_{\mathrm{f}}(z,t) \quad \text{for all } (z,t). \end{aligned} \tag{2.10}$$

It is convenient to describe the evolution of these components by a vector of percentages $\boldsymbol{p} = \boldsymbol{p}(z,t)$, where we assume that

$$\phi_{\mathrm{f}}^{(l)}(z,t) = p^{(l)}(z,t)\phi_{\mathrm{f}}(z,t) \quad \text{for all } (z,t) \text{ and } l = 1,\dots,k_{\mathrm{f}},$$

such that, in light of (2.10),

$$0 \le p^{(l)}(z,t) \le 1 \quad \text{for all } l = 1,\dots,k_{\mathrm{f}}; \quad p^{(1)}(z,t) + \ldots + p^{(k_{\mathrm{f}})}(z,t) = 1 \quad \text{for all } (z,t).$$

Furthermore, we associate with each of the feed streams a percentage vector $\boldsymbol{p}_S = \boldsymbol{p}_S(t)$, where

$$0 \le p_S^{(l)}(t) \le 1 \quad \text{for all } l = 1,\dots,k_{\mathrm{f}}; \quad p_S^{(1)}(t) + \ldots + p_S^{(k_{\mathrm{f}})}(t) = 1 \quad \text{for all } t \in [0,T],\ S \in \{\mathrm{F},\mathrm{W}\}.$$

(It is assumed that no liquid is injected through the gas feed at z_{G}.)

The PDEs that govern the evolution of $\boldsymbol{p}$ are the system of balance equations

$$\partial_t(A(z)\phi_{\mathrm{f}}\boldsymbol{p}) + \partial_z(A(z)\phi_{\mathrm{f}}v_{\mathrm{f}}\boldsymbol{p}) = Q_{\mathrm{F}}(t)\phi_{\mathrm{f,F}}(t)\boldsymbol{p}_{\mathrm{F}}(t)\delta(z - z_{\mathrm{F}}) + Q_{\mathrm{W}}(t)\phi_{\mathrm{f,W}}(t)\boldsymbol{p}_{\mathrm{W}}(t)\delta(z - z_{\mathrm{W}}).$$

The sum of these k_{f} scalar equations yields precisely the third equation in (2.2). From (2.1) and (2.3), we get $q = \phi v_{\mathrm{a}} + \psi v_{\mathrm{s}} + (1 - \phi - \psi)v_{\mathrm{f}}$, which means that

$$\phi_{\mathrm{f}}v_{\mathrm{f}} = (1 - \phi - \psi)v_{\mathrm{f}} = q - \phi v_{\mathrm{a}} - \psi v_{\mathrm{s}}.$$

By the detailed three-phase analysis of [9, Sect. 2.4] and [10, Sect. 3.3], we have also

$$\phi v_{\mathrm{a}} = J(\phi,z,t) - \gamma(z)\partial_z D(\phi), \tag{2.11}$$

$$\psi v_{\mathrm{s}} = -\tilde{F}(\psi,\phi,z,t) + \frac{\gamma(z)\psi}{1-\phi}\partial_z D(\phi), \tag{2.12}$$

and therefore

$$\phi_{\mathrm{f}} v_{\mathrm{f}} = q - J(\phi,z,t) + \tilde{F}(\psi,\phi,z,t) + \gamma(z)\frac{1-\phi-\psi}{1-\phi}\partial_z D(\phi). \tag{2.13}$$

Consequently, we may write the PDE for $\boldsymbol{p}$ as (1.3). The volume fraction of the fluid ϕ_{f} does not appear explicitly in (1.3), since it can be substituted by $\phi_{\mathrm{f}} = 1-\phi-\psi$. The numerical scheme will be based precisely on the formulation (1.3), so we do not further decompose the transport term (2.13).

2.5. **Choice of percentages to describe bias flow and desliming.** In the context of the study of desliming and the effect of the wash water, we find distinguish between the following $k_{\mathrm{f}} = 4$ components of the fluid volume fraction: the water that initially fills the flotation column (volume fraction $\phi_{\mathrm{f}}^{(1)}$), slimes, that is fine solid particles transported with the fluid ($\phi_{\mathrm{f}}^{(2)}$), feed water ($\phi_{\mathrm{f}}^{(3)}$), and wash water ($\phi_{\mathrm{f}}^{(4)}$). The quantities $\phi_{\mathrm{f,F}}^{(i)} = \phi_{\mathrm{f,F}}^{(i)}(t)$, $\phi_{\mathrm{f,W}}^{(i)} = \phi_{\mathrm{f,W}}^{(i)}(t)$, and $\phi_{\mathrm{f,0}}^{(i)} = \phi_{\mathrm{f,0}}^{(i)}(z)$, $i = 1,\dots,4$ describe the corresponding volume fractions in the feed inflow, wash water inflow, and initial fluid volume fraction, respectively. The corresponding percentage vectors are $\boldsymbol{p}_{\mathrm{F}} = \boldsymbol{p}_{\mathrm{F}}(t)$, $\boldsymbol{p}_{\mathrm{W}} = \boldsymbol{p}_{\mathrm{W}}(t)$, and $\boldsymbol{p}_0 = \boldsymbol{p}_0(z)$. In light of the comments made above, we assume

$$\boldsymbol{p}_0(z) = \big(p_0^{(1)}(z), 1-p_0^{(1)}(z), 0, 0\big)^{\mathrm{T}}, \quad 0 \le p_0^{(1)}(z) \le 1, \quad z \in \mathbb{R},$$

i.e., initially, the unit is full of water with possibly a fraction of slimes,

$$\boldsymbol{p}_{\mathrm{F}}(t) = \big(0, 1-p_{\mathrm{F}}^{(3)}(t), p_{\mathrm{F}}^{(3)}(t), 0\big)^{\mathrm{T}}, \quad 0 \le p_{\mathrm{F}}^{(3)}(t) \le 1, \quad t \ge 0,$$

which corresponds to the composition of the feed liquid that may carry slimes, and

$$\boldsymbol{p}_{\mathrm{W}}(t) = (0,0,0,1)^{\mathrm{T}}, \quad t \ge 0,$$

which means that the wash water does not carry any slimes.

3. Numerical scheme

3.1. **Numerical scheme for the aggregate and solid phases.** The spatial discretization of the flotation column is shown in Figure 4 with the constant spatial mesh width $\Delta z := z_i - z_{i-1}$ for each cell interval $I_{i-1/2} := [z_{i-1}, z_i]$. With $z_{i-1/2}$ denoting the midpoint of cell i, we also define $I_i := [z_{i-1/2}, z_{i+1/2}]$. The cross-sectional area is discretized by

$$A_{i-1/2} := \frac{1}{\Delta z}\int_{I_{i-1/2}} A(z)\,\mathrm{d}z, \quad A_i := \frac{1}{\Delta z}\int_{I_i} A(z)\,\mathrm{d}z. \tag{3.1}$$

The initial conditions are discretized by

$$\phi_{i-1/2}^0 = \frac{1}{A_{i-1/2}\Delta z}\int_{I_{i-1/2}} \phi(z,0)A(z)\,\mathrm{d}z, \quad \psi_{i-1/2}^0 = \frac{1}{A_{i-1/2}\Delta z}\int_{I_{i-1/2}} \psi(z,0)A(z)\,\mathrm{d}z, \quad i = 1,\dots,N. \tag{3.2}$$

In what follows, we define the forward and backward spatial difference operators $\Delta_+ a_i := a_{i+1} - a_i$ and $\Delta_- a_i := a_i - a_{i-1}$, as well as $a^+ := \max\{a,0\}$, $a^- := \min\{a,0\}$, and

$$\gamma_i := \gamma(z_i), \quad q_i^{n,\pm} := q(z_i,t^n)^{\pm}, \quad Q_i^{n,\pm} := A_i q_i^{n,\pm}, \quad \text{etc.}, \quad \text{for } i \in \mathbb{Z}.$$

Furthermore, we define the function by $\hat{v}(\phi) := \tilde{v}(\phi)/(1-\phi)$, which is bounded on $[0,1]$ (due to kinematic relations outlined e.g. in [9]); for instance, if $\tilde{v}(\phi)$ is given by (2.7), then $\|\hat{v}\|_\infty = v_{\mathrm{term}}$.

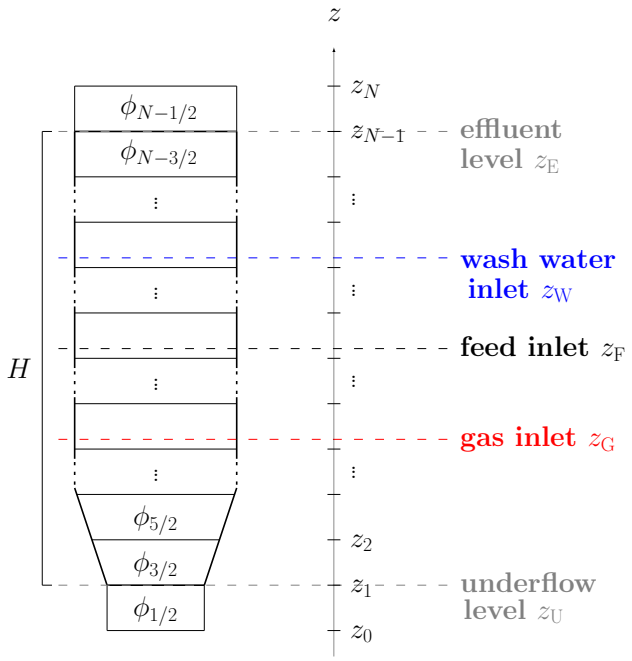

FIGURE 4. Grid for the discretization of the flotation column.

The simulation is done over N_T time steps until a final time $T = N_T \Delta t$, where the fixed time step Δt is chosen such that the CFL condition

$$\frac{\Delta t}{\Delta z}\left(\frac{2\|Q\|_{\infty,T}}{A_{\min}} + M_1\|\tilde{v}'\|_\infty + \beta_1(\Delta z)\right) \le 1 \tag{CFL}$$

is satisfied, where

$$A_{\min} \coloneqq \min_{i=1,\dots,N} A_i, \quad \|Q\|_{\infty,T} \coloneqq \max_{0\le t\le T}\big(Q_F(t) + Q_W(t) + Q_G(t)\big),$$
$$M_1 \coloneqq \max_{i\in\{2,\dots,N\}}\left\{\frac{A_i}{A_{i-1/2}}, \frac{A_{i-1}}{A_{i-1/2}}\right\}, \quad \beta_1 \coloneqq 2M_1\left(\|q\|_\infty + \|\tilde{v}_{\mathrm{hs}}\|_\infty + \|\tilde{v}'_{\mathrm{hs}}\|_\infty + \|\hat{v}\|_\infty + \frac{\|d\|_\infty}{\Delta z}\right).$$

The first equation in (1.1) depends on ϕ only. The total numerical flux for ϕ associated with the cell interface $z = z_i$ at time $t = t^n$ is given by

$$\Phi_i^n \coloneqq \begin{cases} \phi_{1/2}^n q_0^{n,-} & \text{for } i = 0, \\ \phi_{i-1/2}^n q_i^{n,+} + \phi_{i+1/2}^n q_i^{n,-} + \gamma_i \phi_{i-1/2}^n \tilde{v}\big(\phi_{i+1/2}^n\big) - \dfrac{\gamma_i}{\Delta z}\Delta_+ D\big(\phi_{i-1/2}^n\big) & \text{for } i = 1,\dots,N-1, \\ \phi_{N-1/2}^n q_N^{n,+} & \text{for } i = N, \end{cases} \tag{3.3}$$

where we recall that $\tilde{v} = \tilde{v}(\phi)$ is given by (2.7). Since the bulk fluxes above and below the column are directed away from it, $\phi_{i-1/2}^n q_0^{n+} = 0$ and $\phi_{N+1/2}^n q_N^{n-} = 0$ for any values of $\phi_{i-1/2}^n$ and $\phi_{N+1/2}^n$. To simplify the presentation, we use the formula for the case $i = 1,\dots,N-1$ in (3.3) as the definition of Φ_i^n for all i along with setting $\phi_{-1/2}^n \coloneqq 0$ and $\phi_{N+1/2}^n \coloneqq 0$. Furthermore, we set $\lambda \coloneqq \Delta t/\Delta z$.

Then the marching formula for advancing the numerical solution for ϕ from $t = t^n$ to t^{n+1} is

$$\begin{aligned}\phi_{i-1/2}^{n+1} &= \phi_{i-1/2}^n - \frac{\lambda}{A_{i-1/2}}\big(\Delta_-(A_i\Phi_i^n) - Q_{\mathrm{F}}^n\phi_{\mathrm{F}}^n\delta_{\mathrm{F},i-1/2} - Q_{\mathrm{G}}^n\phi_{\mathrm{G}}^n\delta_{\mathrm{G},i-1/2}\big)\\ &= \phi_{i-1/2}^n - \frac{\lambda}{A_{i-1/2}}\bigg(\Delta_-\big(\phi_{i-1/2}^n Q_i^{n+}\big) + \Delta_-\big(\phi_{i+1/2}^n Q_i^{n-}\big) + \Delta_-\big((A\gamma)_i\phi_{i-1/2}^n\tilde{v}\big(\phi_{i+1/2}^n\big)\big)\\ &\quad - \Delta_-\bigg(\frac{(A\gamma)_i}{\Delta z}\Delta_+ D\big(\phi_{i-1/2}^n\big)\bigg) - Q_{\mathrm{F}}^n\phi_{\mathrm{F}}^n\delta_{\mathrm{F},i-1/2} - Q_{\mathrm{G}}^n\phi_{\mathrm{G}}^n\delta_{\mathrm{G},i-1/2}\bigg).\end{aligned} \tag{3.4}$$

The total numerical flux for ψ is given by

$$\begin{aligned}\Psi_i^n &\coloneqq \psi_{i-1/2}^n q_i^{n+} + \psi_{i+1/2}^n q_i^{n-} + \gamma_i\bigg(G_i^n\big(\psi_{i-1/2}^n, \psi_{i+1/2}^n\big)\\ &\quad + \frac{\psi_{i+1/2}^n}{1-\phi_{i+1/2}^n}\bigg(-\phi_{i-1/2}^n\tilde{v}\big(\phi_{i+1/2}^n\big) + \frac{(\Delta_+ D(\phi_{i-1/2}^n))^-}{\Delta z}\bigg) + \frac{\psi_{i-1/2}^n}{1-\phi_{i-1/2}^n}\frac{(\Delta_+ D(\phi_{i-1/2}^n))^+}{\Delta z}\bigg),\end{aligned} \tag{3.5}$$

where we set $\psi_{-1/2}^n \coloneqq 0$ and $\psi_{N+1/2}^n \coloneqq 0$ with the same motivation as for ϕ above (these values are irrelevant) and $G_i^n(\psi_{i-1/2}^n, \psi_{i+1/2}^n)$ is the Engquist–Osher numerical flux [22] associated with the function

$$f_{\mathrm{b},i}^n(\psi) \coloneqq -\psi\tilde{v}_{\mathrm{hs}}(\psi/\psi_{\max,i}^n), \quad \tilde{v}_{\mathrm{hs}}(u) \coloneqq \begin{cases} v_{\mathrm{hs}}(u) & \text{for } u < 1,\\ 0 & \text{for } u > 1,\end{cases} \tag{3.6}$$

where we define

$$\psi_{\max,i}^n \coloneqq \min\big\{1-\phi_{i-1/2}^n, 1-\phi_{i+1/2}^n\big\} = 1 - \max\big\{\phi_{i-1/2}^n, \phi_{i+1/2}^n\big\}, \tag{3.7}$$

and recall that $v_{\mathrm{hs}} \geq 0$ is given by (2.6) and the minus sign appears in (3.6) since we expect particles to settle downward.

For later use, we recall from [11] an (easily proven) scaling property.

Lemma 3.1. *Assume that ω and $\tilde{\omega}$ are the unique local maximum and inflection point, respectively, of $[0,1] \ni u \mapsto f(u) \coloneqq uv_{\mathrm{hs}}(u)$ (cf. (3.6)). Then $\hat{\psi}_i^n = \omega\psi_{\max,i}^n$ for all i and n and all possible values $0 \leq \psi_{\max,i}^n \leq 1$. Moreover, the unique inflection point $\psi_{\mathrm{infl},i}^n \in (\hat{\psi}_i^n, \psi_{\max,i}^n)$ satisfies $\psi_{\mathrm{infl},i}^n = \tilde{\omega}\psi_{\max,i}^n$ for all i and n and all possible values $0 \leq \psi_{\max,i}^n \leq 1$.*

Proof. See [11, Lemma 3.1]. □

For the implementation and later analysis, we use that

$$G_i^n\big(\psi_{i-1/2}^n, \psi_{i+1/2}^n\big) = G_i^{n,+}\big(\psi_{i-1/2}^n\big) + G_i^{n,-}\big(\psi_{i+1/2}^n\big), \tag{3.8}$$

where by utilizing that $f_{\mathrm{b},i}^n$ has a unique minimum at $\hat{\psi}_i^n$,

$$\begin{aligned} G_i^{n,+}\big(\psi_{i-1/2}^n\big) &\coloneqq \int_0^{\psi_{i-1/2}^n} \max\big\{0, (f_{\mathrm{b},i}^n)'(s)\big\}\,\mathrm{d}s = \begin{cases} 0 & \text{if } \psi_{i-1/2}^n \leq \hat{\psi}_i^n,\\ f_{\mathrm{b},i}^n(\psi_{i-1/2}^n) - f_{\mathrm{b},i}^n(\hat{\psi}_i^n) & \text{if } \psi_{i-1/2}^n > \hat{\psi}_i^n,\end{cases}\\ G_i^{n,-}\big(\psi_{i+1/2}^n\big) &\coloneqq \int_0^{\psi_{i+1/2}^n} \min\big\{0, (f_{\mathrm{b},i}^n)'(s)\big\}\,\mathrm{d}s = \begin{cases} f_{\mathrm{b},i}^n(\psi_{i+1/2}^n) & \text{if } \psi_{i+1/2}^n \leq \hat{\psi}_i^n,\\ f_{\mathrm{b},i}^n(\hat{\psi}_i^n) & \text{if } \psi_{i+1/2}^n > \hat{\psi}_i^n.\end{cases}\end{aligned} \tag{3.9}$$

The marching formula for advancing the numerical solution for ψ from $t = t^n$ to t^{n+1} now becomes

$$\begin{aligned}\psi_{i-1/2}^{n+1} &= \psi_{i-1/2}^{n} - \frac{\lambda}{A_{i-1/2}}\big(\Delta_-(A_i\Psi_i^n) - Q_{\mathrm{F}}^n\psi_{\mathrm{F}}^n\delta_{\mathrm{F},i-1/2}\big)\\ &= \psi_{i-1/2}^{n} - \frac{\lambda}{A_{i-1/2}}\bigg(\Delta_-\big(\psi_{i-1/2}^nQ_i^{n+}\big) + \Delta_-\big(\psi_{i+1/2}^nQ_i^{n-}\big)\\ &\quad + \Delta_-\bigg((A\gamma)_i\bigg(G_i^n\big(\psi_{i-1/2}^n,\psi_{i+1/2}^n\big) + \frac{\psi_{i+1/2}^n}{1-\phi_{i+1/2}^n}\bigg(-\phi_{i-1/2}^n\tilde{v}\big(\phi_{i+1/2}^n\big) + \frac{(\Delta_+D(\phi_{i-1/2}^n))^-}{\Delta z}\bigg)\\ &\quad + \frac{\psi_{i-1/2}^n}{1-\phi_{i-1/2}^n}\frac{(\Delta_+D(\phi_{i-1/2}^n))^+}{\Delta z}\bigg)\bigg) - Q_{\mathrm{F}}^n\psi_{\mathrm{F}}^n\delta_{\mathrm{F},i-1/2}\bigg).\end{aligned} \tag{3.10}$$

By a slight modification of the proofs of [10, Theorems 5.1 and 5.3] we may prove the following lemma.

Lemma 3.2. *Assume that the CFL condition (CFL) is in effect and the initial data for ϕ satisfy $0 \le \phi(z,0) \le 1$, then the ϕ-scheme (3.4) is monotone and produces approximate solutions that satisfy*

$$0 \le \phi_{i-1/2}^n \le 1 \quad \text{for all } i = 1,\dots,N \text{ and } n = 1,\dots,N_T.$$

If the initial data for ψ satisfy $0 \le \psi(z,0) \le 1-\phi(z,0)$ and the feed volume fraction $\psi_{\mathrm{F}}(t) \le 1-\phi_{\mathrm{F}}(t)$, then the marching formula of the ψ-scheme (3.10) monotone and combined with (3.4) produces approximate solutions that satisfy

$$0 \le \psi_{i-1/2}^n \le 1-\phi_{i-1/2}^n \quad \text{for all } i = 1,\dots,N \text{ and } n = 1,\dots,N_T.$$

3.2. **Numerical scheme for the liquid components.** The sum of the marching formulas for ϕ and ψ, (3.4) and (3.10),

$$\begin{aligned}\phi_{i-1/2}^{n+1} + \psi_{i-1/2}^{n+1} &= \phi_{i-1/2}^{n} + \psi_{i-1/2}^{n}\\ &\quad - \frac{\lambda}{A_{i-1/2}}\Big(\Delta_-\big(A_i(\Phi_i^n+\Psi_i^n)\big) - Q_{\mathrm{F}}^n(\phi_{\mathrm{F}}^n+\psi_{\mathrm{F}}^n)\delta_{\mathrm{F},i-1/2} - Q_{\mathrm{G}}^n\phi_{\mathrm{G}}^n\delta_{\mathrm{G},i-1/2}\Big),\end{aligned}$$

can be written as

$$\begin{aligned}1-\phi_{i-1/2}^{n+1} - \psi_{i-1/2}^{n+1} &= 1-\phi_{i-1/2}^{n} - \psi_{i-1/2}^{n}\\ &\quad - \frac{\lambda}{A_{i-1/2}}\Big(\Delta_-\big(A_i(-\Phi_i^n-\Psi_i^n)\big) + Q_{\mathrm{F}}^n(\phi_{\mathrm{F}}^n+\psi_{\mathrm{F}}^n)\delta_{\mathrm{F},i-1/2} + Q_{\mathrm{G}}^n\phi_{\mathrm{G}}^n\delta_{\mathrm{G},i-1/2}\Big).\end{aligned}$$

If we define the local fluid volume fraction $\phi_{\mathrm{f},i-1/2}^n \coloneqq 1-\phi_{i-1/2}^n-\psi_{i-1/2}^n$ and consistently with (2.11)–(2.13), the numerical flux $\Phi_{\mathrm{f},i}^n \coloneqq q_i^n - \Phi_i^n - \Psi_i^n$, then we obtain

$$\begin{aligned}\phi_{\mathrm{f},i-1/2}^{n+1} &= \phi_{\mathrm{f},i-1/2}^{n}\\ &\quad - \frac{\lambda}{A_{i-1/2}}\big(\Delta_-(A_i\Phi_{\mathrm{f},i}^n) + Q_{\mathrm{F}}^n(1-\phi_{\mathrm{f,F}}^n)\delta_{\mathrm{F},i-1/2} + Q_{\mathrm{G}}^n(1-\phi_{\mathrm{f,G}}^n)\delta_{\mathrm{G},i-1/2} - \Delta_-(A_iq_i^n)\big).\end{aligned}$$

Taking into account that

$$-\Delta_-(A_iq_i) = \begin{cases} -Q_S^n & \text{if } \delta_{S,i-1/2} = 1,\ S \in \{\mathrm{F},\mathrm{G},\mathrm{W}\},\\ 0 & \text{otherwise,}\end{cases}$$

and $\phi^n_{\mathrm{f,W}} = 1$, we get

$$\phi^{n+1}_{\mathrm{f},i-1/2} = \phi^n_{\mathrm{f},i-1/2} - \frac{\lambda}{A_{i-1/2}}\big(\Delta_-(A_i\Phi^n_{\mathrm{f},i}) - Q^n_{\mathrm{F}}\phi^n_{\mathrm{f,F}}\delta_{\mathrm{F},i-1/2} - Q^n_{\mathrm{G}}\phi^n_{\mathrm{f,G}}\delta_{\mathrm{G},i-1/2} - Q^n_{\mathrm{W}}\phi^n_{\mathrm{f,W}}\delta_{\mathrm{W},i-1/2}\big). \tag{3.11}$$

Based on (3.11) and the explicit percentage propagation scheme proposed in [8], and utilizing the upwind operator $\mathrm{Upw}(a;b,c) \coloneqq \max\{a,0\}b + \min\{a,0\}c$, we get the scheme

$$\begin{aligned}\boldsymbol{p}^{n+1}_{i-1/2}\phi^{n+1}_{\mathrm{f},i-1/2} = \boldsymbol{p}^n_{i-1/2}\phi^n_{\mathrm{f},i-1/2} - \frac{\lambda}{A_{i-1/2}}\Big(&\Delta_-\big(A_i\,\mathrm{Upw}(\Phi^n_{\mathrm{f},i};\boldsymbol{p}^n_{i-1/2},\boldsymbol{p}^n_{i+1/2})\big)\\ &- Q^n_{\mathrm{F}}\boldsymbol{p}^n_{\mathrm{F}}\phi^n_{\mathrm{f,F}}\delta_{\mathrm{F},i-1/2} - Q^n_{\mathrm{G}}\boldsymbol{p}^n_{\mathrm{G}}\phi^n_{\mathrm{f,G}}\delta_{\mathrm{G},i-1/2} - Q^n_{\mathrm{W}}\boldsymbol{p}^n_{\mathrm{W}}\phi^n_{\mathrm{f,W}}\delta_{\mathrm{W},i-1/2}\big)\Big)\end{aligned} \tag{3.12}$$

for the update of the percentage vectors $\boldsymbol{p}^n_{i-1/2}$. This scheme delivers $\boldsymbol{p}^{n+1}_{i-1/2}$ whenever $\phi^{n+1}_{\mathrm{f},i-1/2} > 0$; in the possible case that $\phi^{n+1}_{\mathrm{f},i-1/2} = 0$, we set

$$\boldsymbol{p}^{n+1}_{i-1/2} \coloneqq \boldsymbol{p}^n_{i-1/2} \tag{3.13}$$

From (3.3) and (3.5) we deduce that the numerical flux $\Phi^n_{\mathrm{f},i}$ is explicitly given by

$$\begin{aligned}\Phi^n_{\mathrm{f},i} &= q^n_i - \Big(\phi^n_{i-1/2}q^{n+}_i + \phi^n_{i+1/2}q^{n-}_i + \gamma_i\phi^n_{i-1/2}\tilde{v}\big(\phi^n_{i+1/2}\big) - \frac{\gamma_i}{\Delta z}\Delta_+D\big(\phi^n_{i-1/2}\big)\Big)\\
&\quad - \Bigg(\psi^n_{i-1/2}q^{n+}_i + \psi^n_{i+1/2}q^{n-}_i + \gamma_i\Bigg(G^n_i\big(\psi^n_{i-1/2},\psi^n_{i+1/2}\big)\\
&\quad + \frac{\psi^n_{i+1/2}}{1-\phi^n_{i+1/2}}\Bigg(-\phi^n_{i-1/2}\tilde{v}\big(\phi^n_{i+1/2}\big) + \frac{(\Delta_+D(\phi^n_{i-1/2}))^-}{\Delta z}\Bigg) + \frac{\psi^n_{i-1/2}}{1-\phi^n_{i-1/2}}\frac{(\Delta_+D(\phi^n_{i-1/2}))^+}{\Delta z}\Bigg)\Bigg)\\
&= \big(1-\phi^n_{i-1/2}-\psi^n_{i-1/2}\big)q^{n,+}_i + \big(1-\phi^n_{i+1/2}-\psi^n_{i+1/2}\big)q^{n,-}_i\\
&\quad - \gamma_i\Bigg(\phi^n_{i-1/2}\tilde{v}\big(\phi^n_{i+1/2}\big) - \frac{\Delta_+D(\phi^n_{i-1/2})}{\Delta z} + G^n_i\big(\psi^n_{i-1/2},\psi^n_{i+1/2}\big)\\
&\quad + \frac{\psi^n_{i+1/2}}{1-\phi^n_{i+1/2}}\Bigg(-\phi^n_{i-1/2}\tilde{v}\big(\phi^n_{i+1/2}\big) + \frac{(\Delta_+D(\phi^n_{i-1/2}))^-}{\Delta z}\Bigg) + \frac{\psi^n_{i-1/2}}{1-\phi^n_{i-1/2}}\frac{(\Delta_+D(\phi^n_{i-1/2}))^+}{\Delta z}\Bigg)\\
&= \phi^n_{\mathrm{f},i-1/2}q^{n,+}_i + \phi^n_{\mathrm{f},i+1/2}q^{n,-}_i - \gamma_i\Bigg(\frac{1-\phi^n_{i+1/2}-\psi^n_{i+1/2}}{1-\phi^n_{i+1/2}}\phi^n_{i-1/2}\tilde{v}\big(\phi^n_{i+1/2}\big) + G^n_i\big(\psi^n_{i-1/2},\psi^n_{i+1/2}\big)\\
&\quad - \frac{1-\phi^n_{i+1/2}-\psi^n_{i+1/2}}{1-\phi^n_{i+1/2}}\frac{(\Delta_+D(\phi^n_{i-1/2}))^-}{\Delta z} - \frac{1-\phi^n_{i-1/2}-\psi^n_{i-1/2}}{1-\phi^n_{i-1/2}}\frac{(\Delta_+D(\phi^n_{i-1/2}))^+}{\Delta z}\Bigg).\end{aligned}$$

Thus, we finally get

$$\begin{aligned}\Phi^n_{\mathrm{f},i} = \phi^n_{\mathrm{f},i-1/2}q^{n,+}_i + \phi^n_{\mathrm{f},i+1/2}q^{n,-}_i + \gamma_i\Bigg(&-\frac{\phi^n_{i-1/2}\tilde{v}(\phi^n_{i+1/2})}{1-\phi^n_{i+1/2}}\phi^n_{\mathrm{f},i+1/2} - G^n_i\big(\psi^n_{i-1/2},\psi^n_{i+1/2}\big)\\
&+ \frac{(\Delta_+D(\phi^n_{i-1/2}))^-}{\Delta z(1-\phi^n_{i+1/2})}\phi^n_{\mathrm{f},i+1/2} + \frac{(\Delta_+D(\phi^n_{i-1/2}))^+}{\Delta z(1-\phi^n_{i-1/2})}\phi^n_{\mathrm{f},i-1/2}\Bigg).\end{aligned} \tag{3.14}$$

To be able to invoke arguments akin to those of the proofs of Lemmas 3.2 and 3.4 of [8] in order to prove that the numerical percentages determined via (3.10) are all non-negative, we first prove the following lemma related to one particular term in the right-hand side of (3.14).

Lemma 3.3. *Assume that the CFL condition (CFL) is in effect and $G_i^n(\psi_{i-1/2}^n, \psi_{i+1/2}^n)$ denotes the Engquist–Osher numerical flux as defined by (3.6) to (3.9). Then we may write*

$$\begin{aligned} -G_i^n\big(\psi_{i-1/2}^n, \psi_{i+1/2}^n\big) &= \tilde{G}_i^{n,+}\big(\psi_{i-1/2}^n, \psi_{i+1/2}^n\big)\big(1-\phi_{i-1/2}^n-\psi_{i-1/2}^n\big) \\ &\quad + \tilde{G}_i^{n,-}\big(\psi_{i-1/2}^n, \psi_{i+1/2}^n\big)\big(1-\phi_{i+1/2}^n-\psi_{i+1/2}^n\big) \\ &= \tilde{G}_i^{n,+}\big(\psi_{i-1/2}^n, \psi_{i+1/2}^n\big)\phi_{\mathrm{f},i-1/2}^n + \tilde{G}_i^{n,-}\big(\psi_{i-1/2}^n, \psi_{i+1/2}^n\big)\phi_{\mathrm{f},i+1/2}^n \end{aligned} \tag{3.15}$$

with functions $\tilde{G}_i^{n,+}(\psi_{i-1/2}^n, \psi_{i+1/2}^n) \geq 0$ and $\tilde{G}_i^{n,-}(\psi_{i-1/2}^n, \psi_{i+1/2}^n) \leq 0$ that satisfy

$$\big|\tilde{G}_i^{n,\pm}\big(\psi_{i-1/2}^n, \psi_{i+1/2}^n\big)\big| \leq \|\tilde{v}_{\mathrm{hs}}\|_\infty + \|\tilde{v}_{\mathrm{hs}}'\|_\infty. \tag{3.16}$$

Proof. From (3.9) we obtain

$$-G_i^n(\psi_{i-1/2}^n, \psi_{i+1/2}^n) = \begin{cases} -f_{\mathrm{b},i}^n(\psi_{i+1/2}^n) & \text{if } \psi_{i-1/2}^n, \psi_{i+1/2}^n \hat{\psi}_i^n \text{ (Case1)}, \\ -f_{\mathrm{b},i}^n(\hat{\psi}_i^n) & \text{if } \psi_{i-1/2}^n \leq \hat{\psi}_i^n < \psi_{i+1/2}^n \text{ (Case 2)}, \\ f_{\mathrm{b},i}^n(\hat{\psi}_i^n) - f_{\mathrm{b},i}^n(\psi_{i-1/2}^n) - f_{\mathrm{b},i}^n(\psi_{i+1/2}^n) & \text{if } \psi_{i+1/2}^n \leq \hat{\psi}_i^n < \psi_{i-1/2}^n \text{ (Case 3)}, \\ -f_{\mathrm{b},i}^n(\psi_{i-1/2}^n) & \text{if } \psi_{i-1/2}^n, \psi_{i+1/2}^n > \hat{\psi}_i^n \text{ (Case 4)}. \end{cases}$$

In Case 1, and exploiting that $f_{\mathrm{b},i}^n(1-\phi_{i-1/2}^n) = 0$ as well as that

$$\begin{aligned} 1-\phi_{i-1/2}^n-\psi_{i-1/2}^n &\geq 1-\phi_{i-1/2}^n-\hat{\psi}_i^n = 1-\phi_{i-1/2}^n-\omega\min\big\{1-\phi_{i-1/2}^n, 1-\phi_{i+1/2}^n\big\} \\ &\geq (1-\omega)\big(1-\phi_{i-1/2}^n\big) > 0, \end{aligned}$$

where ω is introduced in Lemma 3.1, we can write

$$\begin{aligned} 0 \leq -\frac{G_i^n(\psi_{i-1/2}^n, \psi_{i+1/2}^n)}{1-\phi_{i-1/2}^n-\psi_{i-1/2}^n} &= -\frac{f_{\mathrm{b},i}^n(\psi_{i+1/2}^n)}{1-\phi_{i-1/2}^n-\psi_{i-1/2}^n} \leq -\frac{f_{\mathrm{b},i}^n(\hat{\psi}_i^n)}{1-\phi_{i-1/2}^n-\hat{\psi}_i^n} \\ = \frac{f_{\mathrm{b},i}^n(1-\phi_{i-1/2}^n) - f_{\mathrm{b},i}^n(\hat{\psi}_i^n)}{1-\phi_{i-1/2}^n-\hat{\psi}_i^n} &= (f_{\mathrm{b},i}^n)'(\xi_{i-1/2}^n), \quad \xi_{i-1/2}^n \in [\hat{\psi}_i^n, 1-\phi_{i-1/2}^n]. \end{aligned}$$

This proves that for Case 1 we may define

$$\tilde{G}_i^{n,+}\big(\psi_{i-1/2}^n, \psi_{i+1/2}^n\big) := -\frac{f_{\mathrm{b},i}^n(\psi_{i+1/2}^n)}{1-\phi_{i-1/2}^n-\psi_{i-1/2}^n} \geq 0, \quad \tilde{G}_i^{n,-}\big(\psi_{i-1/2}^n, \psi_{i+1/2}^n\big) := 0,$$

where

$$\big|\tilde{G}_i^{n,+}\big(\psi_{i-1/2}^n, \psi_{i+1/2}^n\big)\big| \leq \|f_{\mathrm{b},i}^n\|_\infty \leq \|\tilde{v}_{\mathrm{hs}}\|_\infty + \|\tilde{v}_{\mathrm{hs}}'\|_\infty. \tag{3.17}$$

The same discussion also handles Case 2, for which we may choose

$$\tilde{G}_i^{n,+}\big(\psi_{i-1/2}^n, \psi_{i+1/2}^n\big) := -\frac{f_{\mathrm{b},i}^n(\hat{\psi}_i^n)}{1-\phi_{i-1/2}^n-\psi_{i-1/2}^n} \geq 0, \quad \tilde{G}_i^{n,+}\big(\psi_{i-1/2}^n, \psi_{i+1/2}^n\big) := 0,$$

and (3.17) remains in effect. In Case 3, we define

$$\begin{aligned} \tilde{G}_i^{n,-}(\psi_{i-1/2}^n, \psi_{i+1/2}^n) &:= \frac{f_{\mathrm{b},i}^n(\hat{\psi}_i^n) - f_{\mathrm{b},i}^n(\psi_{i+1/2}^n)}{1-\phi_{i+1/2}^n-\psi_{i+1/2}^n} \leq 0, \\ \tilde{G}_i^{n,+}(\psi_{i-1/2}^n, \psi_{i+1/2}^n) &:= -\frac{f_{\mathrm{b},i}^n(\psi_{i-1/2}^n)}{1-\phi_{i-1/2}^n-\psi_{i-1/2}^n} \geq 0. \end{aligned}$$

In the present case,

$$\begin{aligned}1-\phi^n_{i+1/2}-\psi^n_{i+1/2} &\geq 1-\phi^n_{i+1/2}-\hat\psi^n_i = 1-\phi^n_{i+1/2}-\omega\min\{1-\phi^n_{i-1/2},1-\phi^n_{i+1/2}\}\\ &\geq (1-\omega)\big(1-\phi^n_{i+1/2}\big)>0,\end{aligned}$$

hence, since $f^n_{\mathrm{b},i}(1-\phi^n_{i+1/2})=0$,

$$\begin{aligned}\big|\tilde G^{n,-}_i(\psi^n_{i-1/2},\psi^n_{i+1/2})\big| &= \frac{f^n_{\mathrm{b},i}(\psi^n_{i+1/2})-f^n_{\mathrm{b},i}(\hat\psi^n_i)}{1-\phi^n_{i+1/2}-\psi^n_{i+1/2}} \leq \frac{-f^n_{\mathrm{b},i}(\hat\psi^n_i)}{1-\phi^n_{i+1/2}-\psi^n_{i+1/2}}\\ &\leq \frac{f^n_{\mathrm{b},i}(1-\phi^n_{i+1/2})-f^n_{\mathrm{b},i}(\hat\psi^n_i)}{1-\phi^n_{i+1/2}-\hat\psi^n_i} = (f^n_{\mathrm{b},i})'(\tilde\xi^n_{i+1/2}),\quad \tilde\xi^n_{i+1/2}\in[\hat\psi^n_i,1-\phi^n_{i+1/2}].\end{aligned} \tag{3.18}$$

On the other hand, since $f^n_{\mathrm{b},i}(1-\phi^n_{i-1/2})=0$,

$$\begin{aligned}\tilde G^{n,+}_i(\psi^n_{i-1/2},\psi^n_{i+1/2}) &= \frac{f^n_{\mathrm{b},i}(1-\phi^n_{i-1/2})-f^n_{\mathrm{b},i}(\psi^n_{i-1/2})}{1-\phi^n_{i-1/2}-\psi^n_{i-1/2}}\\ &= (f^n_{\mathrm{b},i})'(\hat\xi^n_{i-1/2}),\quad \hat\xi^n_{i-1/2}\in[\psi^n_{i-1/2},1-\phi^n_{i-1/2}],\end{aligned} \tag{3.19}$$

so by repeating the discussion of Cases 1 and 2, we may deduce from (3.18) and (3.19) that (3.16) also holds in Case 3. Finally, in Case 4 we choose

$$\tilde G^{n,+}_i(\psi^n_{i-1/2},\psi^n_{i+1/2}) = -\frac{f^n_{\mathrm{b},i}(\psi^n_{i-1/2})}{1-\phi^n_{i-1/2}-\psi^n_{i-1/2}} = -\frac{f^n_{\mathrm{b},i}(1-\phi^n_{i-1/2})-f^n_{\mathrm{b},i}(\psi^n_{i-1/2})}{1-\phi^n_{i-1/2}-\psi^n_{i-1/2}}$$

and $\tilde G^{n,-}_i(\psi^n_{i-1/2},\psi^n_{i+1/2})=0$ and apply arguments known from Cases 1 to 3 to conclude that also in Case 4, (3.16) holds. □

For later use we prove the following properties of the numerical flux $\Phi^n_{\mathrm{f},i}$.

Lemma 3.4. *The following inequality holds:*

$$\max\big\{\Phi^{n,+}_{\mathrm{f},i},-\Phi^{n,-}_{\mathrm{f},i-1}\big\} \leq \left(\|q\|_\infty+\|\tilde v_{\mathrm{hs}}\|_\infty+\|\tilde v'_{\mathrm{hs}}\|_\infty+\|\hat v\|_\infty+\frac{\|d\|_\infty}{\Delta z}\right)\phi^n_{\mathrm{f},i-1/2}. \tag{3.20}$$

Proof. From (3.14) and (3.15) we obtain

$$\begin{aligned}\Phi^{n,+}_{\mathrm{f},i} &\leq \left(q^{n,+}_i+\gamma_i\left(\tilde G^{n,+}_i(\psi^n_{i-1/2},\psi^n_{i+1/2})+\frac{(\Delta_+D(\phi^n_{i-1/2}))^+}{\Delta z(1-\phi^n_{i-1/2})}\right)\right)\phi^n_{\mathrm{f},i-1/2},\\ -\Phi^{n,-}_{\mathrm{f},i-1} &\leq \left(q^{n,-}_{i-1}+\gamma_{i-1}\left(\frac{\phi^n_{i-3/2}\tilde v(\phi^n_{i-1/2})}{1-\phi^n_{i-1/2}}-\tilde G^{n,-}_{i-1}(\psi^n_{i-3/2},\psi^n_{i-1/2})-\frac{(\Delta_+D(\phi^n_{i-3/2}))^-}{\Delta z(1-\phi^n_{i-1/2})}\right)\right)\phi^n_{\mathrm{f},i-1/2}.\end{aligned}$$

We observe that

$$\left|\frac{\phi^n_{i-3/2}\tilde v(\phi^n_{i-1/2})}{1-\phi^n_{i-1/2}}\right| = \big|\phi^n_{i-3/2}\hat v\big(\phi^n_{i-1/2}\big)\big| \leq \|\hat v\|_\infty.$$

Furthermore, since $D=D(\phi)$ is nondecreasing, $(\Delta_+D(\phi^n_{i-1/2}))^+=0$ if $\phi^n_{i+1/2}\leq\phi^n_{i-1/2}$ and

$$\frac{(\Delta_+D(\phi^n_{i-1/2}))^+}{\Delta z(1-\phi^n_{i-1/2})} = \frac{1}{\Delta z}\frac{D(\phi^n_{i+1/2})-D(\phi^n_{i-1/2})}{1-\phi^n_{i-1/2}} \leq \frac{1}{\Delta z}\frac{D(1)-D(\phi^n_{i-1/2})}{1-\phi^n_{i-1/2}} \leq \frac{\|d\|_\infty}{\Delta z}$$

if $\phi^n_{i+1/2} > \phi^n_{i-1/2}$. By analogous reasoning we also get

$$-\frac{(\Delta_+ D(\phi^n_{i-3/2}))^-}{\Delta z(1-\phi^n_{i-1/2})} \le \frac{\|d\|_\infty}{\Delta z}.$$

Utilizing these estimates and (3.16), we finally get

$$\Phi^{n,+}_{\mathrm{f},i} \le \left(\|q\|_\infty + \|\tilde v_{\mathrm{hs}}\|_\infty + \|\tilde v'_{\mathrm{hs}}\|_\infty + \frac{\|d\|_\infty}{\Delta z}\right)\phi^n_{\mathrm{f},i-1/2},$$
$$-\Phi^{n,-}_{\mathrm{f},i-1} \le \left(\|q\|_\infty + \|\tilde v_{\mathrm{hs}}\|_\infty + \|\tilde v'_{\mathrm{hs}}\|_\infty + \|\hat v\|_\infty + \frac{\|d\|_\infty}{\Delta z}\right)\phi^n_{\mathrm{f},i-1/2}.$$

□

Lemma 3.5. *If the CFL condition (CFL) is in effect and for some $n \in \{0,\dots,N_T-1\}$,*

$$p^{(l),n}_{i-1/2} \ge 0 \quad \text{for all } l = 1,\dots,k_{\mathrm{f}} \text{ and } i = 1,\dots,N, \tag{3.21}$$
$$p^{(1),n}_{i-1/2} + \cdots + p^{(k_{\mathrm{f}}),n}_{i-1/2} = 1 \quad \text{for all } i = 1,\dots,N, \tag{3.22}$$

and analogous properties hold for the feed percentage vectors $\boldsymbol{p}^n_S$, $S \in \{\mathrm{F},\mathrm{G},\mathrm{W}\}$, then the percentage vectors

$$\boldsymbol{p}^{n+1}_{i-1/2} = \big(p^{(1),n+1}_{i-1/2},\dots,p^{(k_{\mathrm{f}}),n+1}_{i-1/2}\big)^{\mathrm{T}}$$

defined by (3.12) satisfy

$$p^{(l),n+1}_{i-1/2} \ge 0 \quad \text{for all } l = 1,\dots,k_{\mathrm{f}} \text{ and } i = 1,\dots,N, \tag{3.23}$$
$$p^{(1),n+1}_{i-1/2} + \cdots + p^{(k_{\mathrm{f}}),n+1}_{i-1/2} = 1 \quad \text{for all } i = 1,\dots,N. \tag{3.24}$$

Proof. Assume that (3.22) holds, and select $i \in \{1,\dots,N\}$. If $\phi^{n+1}_{i-1/2} = 0$, then $p^{(l),n+1}_{i-1/2} \ge 0$ follows from (3.13), so let us assume that $\phi^{n+1}_{i-1/2} > 0$. Choose $l \in \{1,\dots,k_{\mathrm{f}}\}$. Then we obtain for the l-th component of (3.12):

$$\begin{aligned}
p^{(l),n+1}_{i-1/2}\phi^{n+1}_{\mathrm{f},i-1/2} &= p^{(l),n}_{i-1/2}\phi^n_{\mathrm{f},i-1/2} - \frac{\lambda}{A_{i-1/2}}\Big(A_i\Phi^{n,+}_{\mathrm{f},i}p^{(l),n}_{i-1/2} + A_i\Phi^{n,-}_{\mathrm{f},i}p^{(l),n}_{i+1/2} - A_{i-1}\Phi^{n,+}_{\mathrm{f},i-1}p^{(l),n}_{i-3/2} \\
&\qquad - A_{i-1}\Phi^{n,-}_{\mathrm{f},i-1}p^{(l),n}_{i-1/2} - Q^n_{\mathrm{F}}p^{(l),n}_{\mathrm{F}}\phi^n_{\mathrm{f,F}}\delta_{\mathrm{F},i-1/2} - Q^n_{\mathrm{G}}p^{(l),n}_{\mathrm{G}}\phi^n_{\mathrm{f,G}}\delta_{\mathrm{G},i-1/2} \\
&\qquad - Q^n_{\mathrm{W}}p^{(l),n}_{\mathrm{W}}\phi^n_{\mathrm{f,W}}\delta_{\mathrm{W},i-1/2}\Big) \\
&\ge p^{(l),n}_{i-1/2}\phi^n_{\mathrm{f},i-1/2} - \frac{\lambda}{A_{i-1/2}}\Big(A_i\Phi^{n,+}_{\mathrm{f},i}p^{(l),n}_{i-1/2} - A_{i-1}\Phi^{n,-}_{\mathrm{f},i-1}p^{(l),n}_{i-1/2}\Big) \\
&\ge \big(\phi^n_{\mathrm{f},i-1/2} - \lambda M_1\big(\Phi^{n,+}_{\mathrm{f},i} - \Phi^{n,-}_{\mathrm{f},i-1}\big)\big)p^{(l),n}_{i-1/2}.
\end{aligned}$$

From Lemma 3.4 we now get

$$p^{(l),n+1}_{i-1/2}\phi^{n+1}_{\mathrm{f},i-1/2} \ge \left\{1 - \lambda 2M_1\left(\|q\|_\infty + \|\tilde v_{\mathrm{hs}}\|_\infty + \|\tilde v'_{\mathrm{hs}}\|_\infty + \|\hat v\|_\infty + \frac{\|d\|_\infty}{\Delta z}\right)\right\}\phi^n_{\mathrm{f},i-1/2}p^{(l),n}_{i-1/2}.$$

Due to the CFL condition, $\{\dots\} > 0$, so if $\phi^{n+1}_{\mathrm{f},i-1/2} > 0$ (the case $\phi^{n+1}_{\mathrm{f},i-1/2} = 0$ is trivial), we conclude that $p^{(l),n+1}_{i-1/2} \ge 0$.

On the other hand, assume that (3.22) holds, and select $i \in \{1,\dots,N\}$. Again, if $\phi^{n+1}_{i-1/2} = 0$, then

$$p^{(1),n+1}_{i-1/2} + \cdots + p^{(k_{\mathrm{f}}),n+1}_{i-1/2} = 1$$

follows from (3.13), so we assume that $\phi^{n+1}_{i-1/2} > 0$. Noticing that

$$\begin{aligned}
&\sum_{l=1}^{k_{\mathrm{f}}} \Delta_-\Big(A_i \operatorname{Upw}\big(\Phi^n_{\mathrm{f},i}; p^{(l),n}_{i-1/2}, p^{(l),n}_{i+1/2}\big)\Big) \\
&= \sum_{l=1}^{k_{\mathrm{f}}} \Big(A_i \Phi^{n,+}_{\mathrm{f},i} p^{(l),n}_{i-1/2} + A_i \Phi^{n,-}_{\mathrm{f},i} p^{(l),n}_{i+1/2} - A_{i-1} \Phi^{n,+}_{\mathrm{f},i-1} p^{(l),n}_{i-3/2} - A_{i-1} \Phi^{n,-}_{\mathrm{f},i-1} p^{(l),n}_{i-1/2}\Big) \\
&= A_i \Phi^{n,+}_{\mathrm{f},i} + A_i \Phi^{n,-}_{\mathrm{f},i} - A_{i-1} \Phi^{n,+}_{\mathrm{f},i-1} - A_{i-1} \Phi^{n,-}_{\mathrm{f},i-1} = \Delta_-(A_i \Phi^n_{\mathrm{f},i}),
\end{aligned}$$

we get by summing the k_{f} scalar equations in (3.11) and taking into account (3.22), along with the analogous properties for the feed percentage vectors $\boldsymbol{p}^n_S$, $S \in \{\mathrm{F}, \mathrm{G}, \mathrm{W}\}$,

$$\begin{aligned}
\phi^{n+1}_{\mathrm{f},i-1/2} \sum_{l=1}^{k_{\mathrm{f}}} p^{(l),n+1}_{i-1/2} = \phi^n_{\mathrm{f},i-1/2} - \frac{\lambda}{A_{i-1/2}} \big(&\Delta_-(A_i \Phi^n_{\mathrm{f},i}) \\
&- Q^n_{\mathrm{F}} \phi^n_{\mathrm{f,F}} \delta_{\mathrm{F},i-1/2} - Q^n_{\mathrm{G}} \phi^n_{\mathrm{f,G}} \delta_{\mathrm{G},i-1/2} - Q^n_{\mathrm{W}} \phi^n_{\mathrm{f,W}} \delta_{\mathrm{W},i-1/2}\big)
\end{aligned}$$

The right-hand side is exactly $\phi^{n+1}_{\mathrm{f},i-1/2}$. Consequently,

$$\phi^{n+1}_{\mathrm{f},i-1/2} \Big(p^{(1),n+1}_{i-1/2} + \cdots + p^{(k_{\mathrm{f}}),n+1}_{i-1/2} - 1\Big) = 0,$$

which implies (3.24) due to the assumption $\phi^{n+1}_{i-1/2} > 0$. □

4. Steady-state analysis

4.1. **Desired steady states.** We are interested in studying the steady-state solutions of (1.1), which depend on the values of the volume fractions at each inlet and the volumetric flows in and out of the column. *Desired* steady states are defined by the following properties.

(1) There is no solid particle (gangue) above the feed level at $z = z_{\mathrm{F}}$, since there is otherwise a risk that it follows the froth upwards and through the effluent. The means that $\psi_3 = \psi_4 = \psi_{\mathrm{E}} = 0$, where ψ_3 and ψ_4 denote the steady-state value of ψ in zone 3 and 4, respectively.
(2) There is no aggregate below the gas inlet at $z = z_{\mathrm{G}}$, so that no aggregate is lost through the underflow; $\phi_1 = \phi_{\mathrm{U}} = 0$, where ϕ_1 denotes the steady-state value of ϕ in zone 1.
(3) There is a stable froth layer above the feed level $z = z_{\mathrm{F}}$, which, to enhance the washing of the foam, fills a part of zone 3; that is, the froth height z_{fr} satisfies $z_{\mathrm{F}} < z_{\mathrm{fr}} < z_{\mathrm{W}}$.
(4) There is a positive bias flow, i.e., the water flow in zone 3 is directed downwards with the purpose of washing entrained gangue particles from the froth: $\phi_{\mathrm{f},3} v_{\mathrm{f}} < 0$.

For the requirements on the volume fraction of aggregates, we recall that only gas is pumped into the column at $z = z_{\mathrm{G}}$; $\phi_{\mathrm{G}} = 1$, and no gas enters elsewhere; $\phi_{\mathrm{F}} = \phi_{\mathrm{W}} = 0$. The wash water inlet contains only clear wash water; $\phi_{\mathrm{f,W}} = 1$ and $\phi_{\mathrm{f,G}} = \phi_{\mathrm{f,F}} = 0$.

4.2. **Conditions on stationary solutions for the aggregates.** A stationary solution $\phi = \phi(z)$ of (1.1) satisfies, in the weak sense,

$$\frac{\mathrm{d}}{\mathrm{d}z}\left(J(\phi, z) - \gamma(z) \frac{\mathrm{d}D(\phi)}{\mathrm{d}z} - q_{\mathrm{G}} H(z - z_{\mathrm{G}})\right) = 0,$$

where H is the Heaviside function. This ODE is equivalent to

$$J(\phi, z) - \gamma(z) d(\phi) \frac{\mathrm{d}\phi(z)}{\mathrm{d}z} - q_{\mathrm{G}} H(z - z_{\mathrm{G}}) = M \quad \text{for all } z, \tag{4.1}$$

where M denotes the constant mass flux per area unit. (This flux cannot have a discontinuity in z by the conservation of mass.) Outside the column, at $z < z_{\mathrm{U}}$ and $z > z_{\mathrm{E}}$, there holds $\gamma(z) = 0$, and in those intervals, (4.1) becomes

$$M = j_{\mathrm{U}}(\phi_{\mathrm{U}}) = -q_{\mathrm{U}}\phi_{\mathrm{U}}, \tag{4.2}$$

$$M = j_{\mathrm{E}}(\phi_{\mathrm{E}}) - q_{\mathrm{G}} = q_{\mathrm{E}}\phi_{\mathrm{E}} - q_{\mathrm{G}}, \tag{4.3}$$

In light of property (2), we require that $\phi_{\mathrm{U}} = 0$, hence (4.2) implies that $M = 0$, and from (4.3) we conclude that the effluent aggregate volume fractionϕ_{E} is given by

$$\phi_{\mathrm{E}} = \frac{q_{\mathrm{G}}}{q_{\mathrm{E}}} = \frac{q_{\mathrm{G}}}{q_{\mathrm{W}} + q_{\mathrm{F}} + q_{\mathrm{G}} - q_{\mathrm{U}}}. \tag{4.4}$$

Based on the constructions made in [5,10], to which we refer for further details, and the definition of desired steady-state solution above, we conclude that $\phi(z) < \phi_{\mathrm{c}}$ for all $z < z_{\mathrm{fr}}$, and Equation (4.1) with $M = 0$ implies that the solution is piecewise constant (since $d(\phi) = 0$ for these ϕ). For $z > z_{\mathrm{fr}}$, the solution $z \mapsto \phi(z)$ is strictly increasing and continuous. This property also holds across $z = z_{\mathrm{W}}$, because of the nonzero term $d(\phi)$, which makes the PDE parabolic. Consequently, we denote such solutions with the subindex 'par'. Thus, the desired steady-state solution is $\phi(z) = \phi_k(z)$ in zone k, $k = 1, \dots, 4$ (see Figure 1), where the subindex refers to the zone number and the constants with a bar are determined below:

$$\begin{aligned}
&\phi_1(z) = 0 \quad \text{for } z_{\mathrm{U}} < z < z_{\mathrm{G}} \text{ (zone 1)},\\
&\phi_2(z) = \bar{\phi}_2 \quad \text{for } z_{\mathrm{G}} < z < z_{\mathrm{F}} \text{ (zone 2)},\\
&\phi_3(z) = \begin{cases} \bar{\phi}_3 & \text{for } z_{\mathrm{F}} < z < z_{\mathrm{fr}},\\ \phi_{3\mathrm{par}}(z) & \text{for } z_{\mathrm{fr}} < z \le z_{\mathrm{W}} \end{cases} \quad \text{(zone 3)},\\
&\phi_4(z) = \phi_{4\mathrm{par}}(z) \quad \text{for } z_{\mathrm{W}} < z \le z_{\mathrm{E}} \text{ (zone 4)}.
\end{aligned} \tag{4.5}$$

This solution satisfies Equation (4.1) with $M = 0$, which yields the following:

$$j_2(\bar{\phi}_2; q_2) - q_{\mathrm{G}} = 0, \qquad \text{jump condition at } z_{\mathrm{G}}, \tag{4.6}$$

$$j_2(\bar{\phi}_2; q_2) = j_3(\bar{\phi}_3; q_3), \quad \text{jump condition at } z_{\mathrm{F}}, \tag{4.7}$$

$$j_3(\phi_3(z); q_3) - d(\phi_3(z))\frac{\mathrm{d}\phi_3(z)}{\mathrm{d}z} - q_{\mathrm{G}} = 0, \qquad \text{in zone 3}, \tag{4.8}$$

$$j_3(\phi_4(z); q_4) - d(\phi_4(z))\frac{\mathrm{d}\phi_4(z)}{\mathrm{d}z} - q_{\mathrm{G}} = 0, \qquad \text{in zone 4}, \tag{4.9}$$

where $\phi_3(z)$ has a discontinuity at $z = z_{\mathrm{fr}}$ from $\phi_3(z_{\mathrm{fr}}^-) = \bar{\phi}_3$ up to the larger value $\phi_3(z_{\mathrm{fr}}^+) = \phi_{\mathrm{c}}$. Furthermore, the solution is continuous at $z = z_{\mathrm{W}}$, hence $\phi_{3\mathrm{par}}(z_{\mathrm{W}}) = \phi_{4\mathrm{par}}(z_{\mathrm{W}})$. The constant solution in zone 2 is the smallest solution $\bar{\phi}_2$ of (4.6) under the constraints

$$q_{\mathrm{G}} \le j_2(\phi_2^{\mathrm{M}}(q_2); q_2), \tag{FIa}$$

$$\bar{\phi}_2 \le \phi_{1\mathrm{Z}}(q_1), \tag{FIb}$$

where ϕ_2^{M} denotes the maximum point of j_2 for given q_2, and $\phi_{1\mathrm{Z}}(q_1)$ is the positive zero of $j_1(\phi; q_1)$; see [10] for exact definitions. Then $\bar{\phi}_3$ is given by (4.7) in $[0, \phi_3^{\mathrm{M}}]$, which implies that $\bar{\phi}_3 < \bar{\phi}_2$ (since $q_{\mathrm{f}} > 0$). No additional condition is necessary for this coupling.

The strictly increasing sub-solutions $\phi_{3\mathrm{par}}(z)$ and $\phi_{4\mathrm{par}}(z)$ satisfy the ODEs given by (4.8) and (4.9), respectively, which we write in the opposite order, since its solutions are obtained from

the initial value at the top:

$$\frac{\mathrm{d}\phi_4}{\mathrm{d}z} = \frac{j_4(\phi_4;q_4)-q_\mathrm{G}}{d(\phi_4)}, \quad z_\mathrm{W} < z < z_\mathrm{E}; \quad \phi_4(z_\mathrm{E}) = \phi_\mathrm{E}, \tag{4.10}$$

$$\frac{\mathrm{d}\phi_3}{\mathrm{d}z} = \frac{j_3(\phi_3;q_3)-q_\mathrm{G}}{d(\phi_3)}, \quad z_\mathrm{fr} < z < z_\mathrm{W}; \quad \phi_3(z_\mathrm{W}) = \phi_4(z_\mathrm{W}). \tag{4.11}$$

The solutions are obtained in the following way. If all bulk velocities are given, then the value ϕ_E is defined by (4.4). Equation (4.10) is solved backwards from z_E to z_W to obtain $\phi_{4\mathrm{par}}(z)$; in particular, the value $\phi_{4\mathrm{par}}(z_\mathrm{W}) = \phi_{3\mathrm{par}}(z_\mathrm{W}) > \phi_\mathrm{c}$ is the starting value for (4.11), which is solved backwards from z_W until the volume fraction $\phi_{3\mathrm{par}}(z)$ reaches down to ϕ_c, which defines the location z_fr. This procedure defines a function $Z_\mathrm{fr}(q_\mathrm{U},q_\mathrm{G},q_\mathrm{F},q_\mathrm{W})$ that gives the froth level z_fr as a function of all bulk velocities. Necessary conditions for the existence of these sub-solutions $\phi_{3\mathrm{par}}(z)$ and $\phi_{4\mathrm{par}}(z)$ are

$$\phi_\mathrm{c} < \phi_\mathrm{E} \le 1 \quad \Leftrightarrow \quad 0 \le -q_\mathrm{U} + q_\mathrm{F} + q_\mathrm{W} < \left(\frac{1}{\phi_\mathrm{c}} - 1\right) q_\mathrm{G}, \tag{Froth1}$$

$$z_\mathrm{F} < z_\mathrm{fr} < z_\mathrm{W} \quad \Leftrightarrow \quad z_\mathrm{F} < Z_\mathrm{fr}(q_\mathrm{U},q_\mathrm{G},q_\mathrm{F},q_\mathrm{W}) < z_\mathrm{W}, \tag{Froth2}$$

$$q_\mathrm{G} < j_3(\phi;q_3) \quad \text{for all } \phi \in (\phi_3^\mathrm{M},\phi_\mathrm{E}) \quad \Leftrightarrow \quad q_\mathrm{G} \begin{cases} < j_3(\phi_{3\mathrm{M}};q_3) & \text{if } \phi_{3\mathrm{M}} < \phi_\mathrm{E}, \\ \le j_3(\phi_\mathrm{E};q_3) & \text{if } \phi_{3\mathrm{M}} \ge \phi_\mathrm{E}. \end{cases} \tag{Froth3}$$

Note that the condition $\phi_{4\mathrm{par}}(z_\mathrm{W}) = \phi_{3\mathrm{par}}(z_\mathrm{W}) > \phi_\mathrm{c}$ is implied by (Froth2), and must be checked in the computer code in order to imply the right inequality of (Froth2). Condition (Froth3) guarantees that the right-hand sides of (4.11) and (4.10) are positive, so that the parabolic solutions are strictly increasing.

For this steady state to be a desirable one, there should also be a positive bias flow in zone 3, which by the definition of the bulk flow q_3 can be written as

$$\phi_{\mathrm{f},3}(z)v_{\mathrm{f},3}(z) = q_3 - \phi_3(z)v_{\mathrm{a},3}(z) - \psi_3(z)v_{\mathrm{s},3}(z) < 0, \tag{4.12}$$

where $v_{\mathrm{a},3}$ and $v_{\mathrm{s},3}$ are the aggregate and solid velocities in zone 3. A desired steady state has $\psi_3 = 0$, and $q_3 = -q_\mathrm{U} + q_\mathrm{G} + q_\mathrm{F}$. At the lower part of zone three, we have $\phi_3(z) = \bar{\phi}_3 < \phi_\mathrm{c}$. Hence, by (4.6) and (4.7) the second term on the right-hand side of (4.12) is $\bar{\phi}_3 v_{\mathrm{a},3}(z) = j_3(\bar{\phi}_3;q_3) = q_\mathrm{G}$. Consequently, (4.12) implies the condition

$$-q_\mathrm{U} + q_\mathrm{F} < 0 \quad \Leftrightarrow \quad q_\mathrm{F} < q_\mathrm{U}. \tag{Bias}$$

The first inequality in (Froth1) and (Bias) imply that $q_\mathrm{F} < q_\mathrm{U} \le q_\mathrm{F} + q_\mathrm{W}$; hence, $q_\mathrm{W} > 0$.

4.3. **Condition on the solids.** For the steady state of the solid phase, we have stated that solids should not move above the feed level. To ensure this, the following conditions must hold; see [10]:

$$f_1(\varphi_1,0) = f_2(\varphi_2,\phi_2) \tag{FJCs}$$

$$q_\mathrm{F}\psi_\mathrm{F} \le f_1(\varphi_1^\mathrm{M},0) \tag{FIas zone 1}$$

$$q_\mathrm{F}\psi_\mathrm{F} \le f_2(\varphi_2^\mathrm{M},\bar{\phi}_2) \tag{FIas zone 2}$$

Note that, since we are supposing $\phi_\mathrm{F} = 0$, then $\psi_\mathrm{F} = \varphi_\mathrm{F}$. The desired steady-state solution for the solids phase is then the following:

$$\begin{aligned} &\psi_1(z) = \bar{\psi}_1, \quad z_\mathrm{U} < z < z_\mathrm{G}, \\ &\psi_2(z) = \bar{\psi}_2 = \frac{\bar{\varphi}_2}{1-\bar{\phi}_2}, \quad z_\mathrm{G} < z < z_\mathrm{F}, \\ &\psi_3(z) = 0, \quad z_\mathrm{F} < z < z_\mathrm{W}, \end{aligned} \tag{4.13}$$

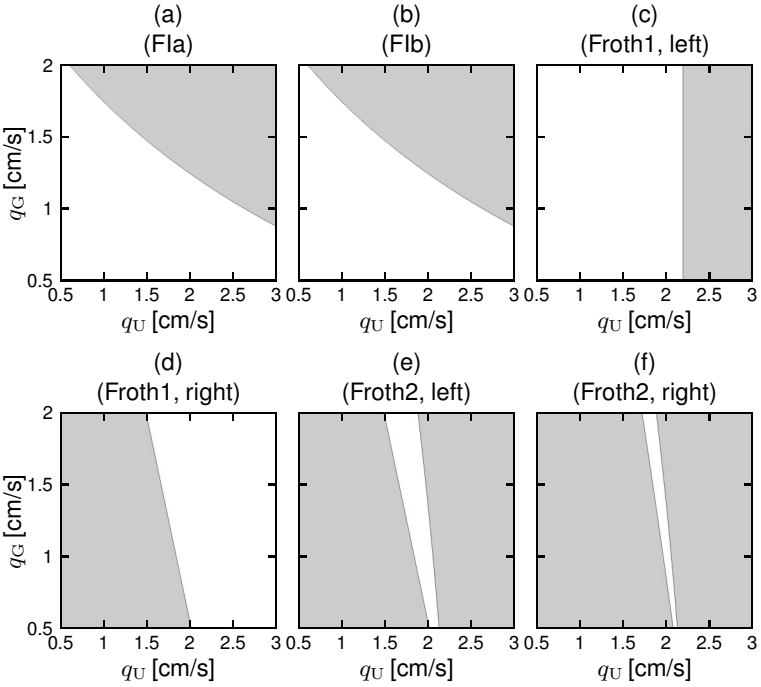

FIGURE 5. Operating charts showing in white the region where each of six conditions is satisfied for fixed values of $q_F = 0.02\,\mathrm{m/s}$ and $q_W = 0.002\,\mathrm{m/s}$.

$$\psi_4(z) = 0, \quad z_W < z \leq z_E.$$

where $\bar{\psi}_1$ and $\bar{\psi}_2$ satisfy the jump condition at z_U and z_G, respectively.

4.4. **Visualization of conditions by operating charts.** The ten necessary conditions (inequalities or equalities) that have to be satisfied for a steady state to be desired are visualized in Figures 5 and 6. The white region represents the values of (q_U, q_G) where the condition is satisfied, for a fixed value of $q_F = 0.02\,\mathrm{m/s}$, $q_W = 0.002\,\mathrm{m/s}$ and $\psi_F = 0.1$, and the values of the parameters stated in Table 1, with $z_E = 2.7025\,\mathrm{m}$. In Figure 6(e), we can see the operating chart whose white region is given by the intersection of all ten conditions. To obtain a desired steady state given by (4.5) and (4.13), it is thus necessary to have a point (q_U, q_G) inside that white region.

In Figure 7, we show the surface $z = Z_{fr}(q_U, q_G, q_F, q_W)$ for fixed (q_F, q_W) and for the values of (q_U, q_G) inside the white region of the operating chart in Figure 6(e). As the contour lines show in Figure 7(c), the depth of the froth below the wash water inlet z_W ranges between 0 and 10 cm.

In Figure 8, we show how the white region of the operating charts evolves with the size of zone 4. As it is shown, the closer the wash water inlet z_w is to the effluent z_E, the larger is the feasible region in the operating charts.

5. NUMERICAL SIMULATIONS

5.1. **Preliminaries.** We simulate the flotation process in a column with height $H = 2.7025\,\mathrm{m}$, with $z_E = 2.7025\,\mathrm{m}$ and the rest of the inlets are located at the heights given in Table 1. We place the wash water inlet really close to the effluent, as wash water is typically sprinkled at the very top of the column. The rest of the parameters are taken as in Table 1.

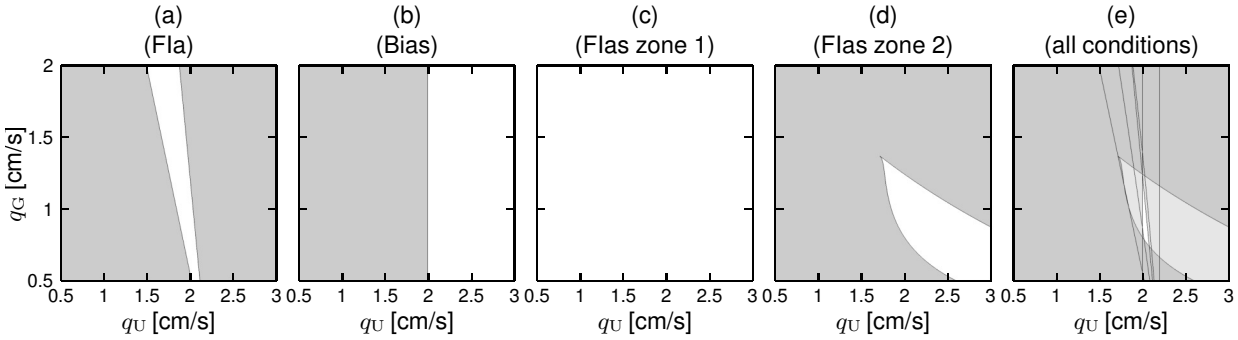

FIGURE 6. Operating charts showing in white the region where each of four conditions is satisfied for fixed values of $q_F = 0.02\,\mathrm{m/s}$ and $q_W = 0.002\,\mathrm{m/s}$. Subplot (e) shows the intersection of all ten conditions.

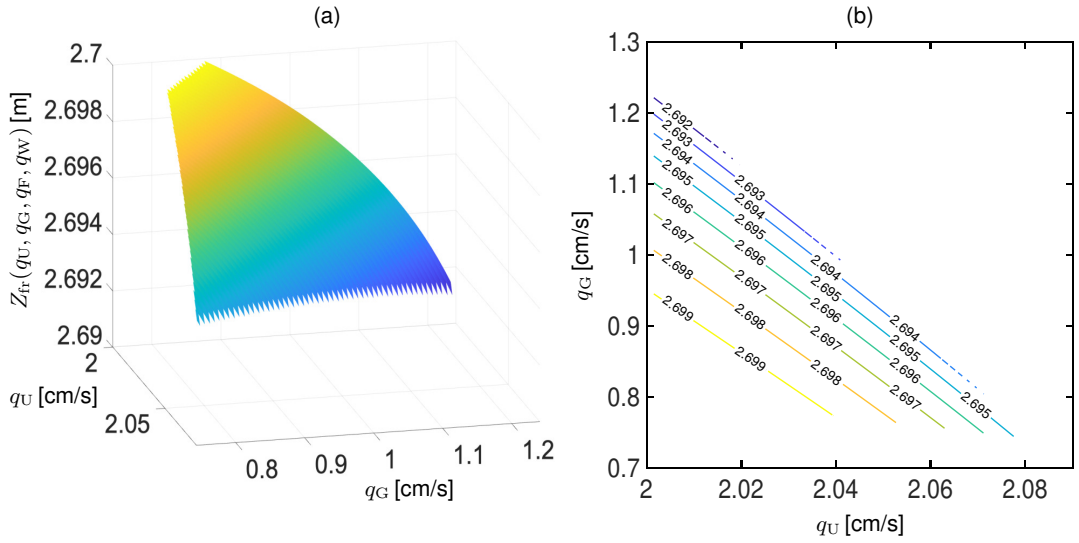

FIGURE 7. Graph of $(q_U, q_G) \mapsto Z_{fr}(q_U, q_G, q_F, q_W)$ and its contours for fixed values $q_F = 0.02\,\mathrm{m/s}$ and $q_W = 0.002\,\mathrm{m/s}$ with column height $H = 2.7025\,\mathrm{m}$.

Throughout this section, the composition of the liquid phase components will be the following: $\boldsymbol{p}_0 = (1, 0, 0, 0)$ is the initial state of the column, $\boldsymbol{p}_F = (0, 0.02, 0.98, 0)$ at the feed inlet, i.e., the feed inlet contains 2% slimes, and $\boldsymbol{p}_W = (0, 0, 0, 1)$ for the wash water inlet.

5.2. **Approximate errors.** To evaluate the accuracy of the numerical scheme, we compute the approximate error

$$\varepsilon_N^{\Delta z}(T) \coloneqq e_N^{\phi}(T) + e_N^{\psi}(T) + \sum_{i=1}^{4} e_N^{\phi_f^{(i)}}(T),$$

where the error for each component is computed by comparing the numerical solution obtained with a spatial discretization with N cells, denoted by $\phi^{\Delta z}(z, t)$, with a reference solution computed

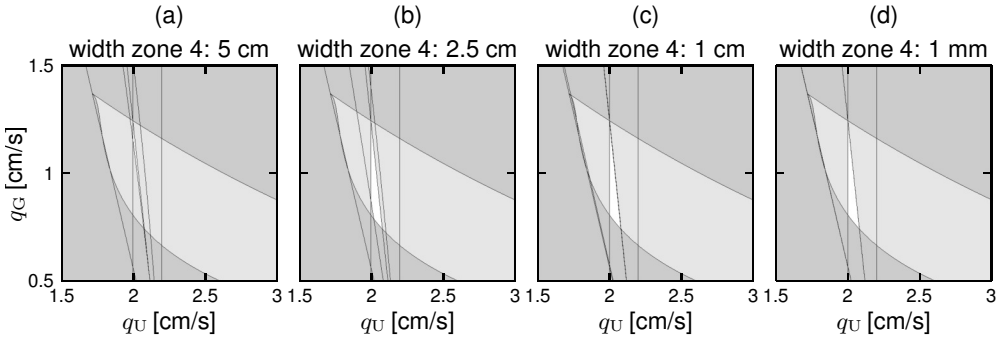

FIGURE 8. Operating charts showing in white the region where all ten conditions are satisfied (cf. Figure 6 (e)) for fixed $q_F = 2\,\mathrm{cm/s}$ and $q_W = 0.2\,\mathrm{cm/s}$ and varying size of zone 4.

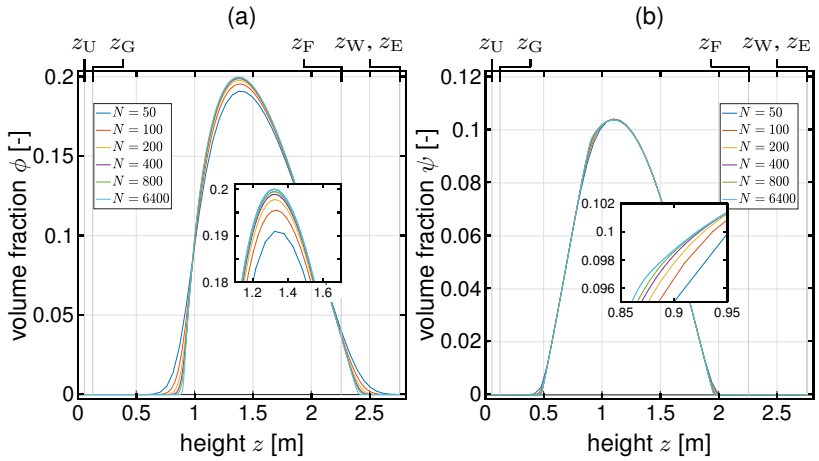

FIGURE 9. Example 1 (accuracy test, smooth solution). Numerical solution for the volume fraction of aggregates ϕ (left) and solids ψ (right) at $T = 4\,\mathrm{s}$ for the sinusoidal initial condition and for different values of N.

with N_{ref} cells, denoted by $\phi^{\Delta z_{\mathrm{ref}}}(z,t)$. Its expression is given by:

$$e_N^{\phi}(T) = \frac{||\phi^{\Delta z}(\cdot,T) - \phi^{\Delta z_{\mathrm{ref}}}(\cdot,T)||}{||\phi^{\Delta z_{\mathrm{ref}}}(\cdot,T)||},$$

with

$$||\phi^{\Delta z}(\cdot,T) - \phi^{\Delta z_{\mathrm{ref}}}(\cdot,T)|| = \sum_{i=0}^{N-1} \Delta z_{\mathrm{ref}} \sum_{k=0}^{m-1} A^{\Delta z_{\mathrm{ref}}}_{im+1/2+k} \left| \phi^{\Delta z}_{i+1/2} - \phi^{\Delta z_{\mathrm{ref}}}_{im+1/2+k} \right|,$$

where $A^{\Delta z_{\mathrm{ref}}}$ is the cross-sectional area (3.1) discretized with N_{ref} cells.

In this work, we will compare the numerical solutions on a sequence of meshes with $N = 50, 100, 200, 400, 800$, and 1600 grid cells, with an approximate reference solution with $N_{\mathrm{ref}} = 6400$. For these meshes, the convergence order is estimated by

$$\Upsilon_N(T) := \log_2(\varepsilon^{\Delta z}_{N/2}(T)/\varepsilon^{\Delta z}_N(T)).$$

TABLE 2. Examples 1 and 2 (accuracy tests): approximate total relative L^1 errors $\varepsilon_N^{\Delta z}(t)$ and estimated orders of convergence $\Upsilon_N(t)$ for Example 1 at $t = 4\,\mathrm{s}$ and Example 2 at $t = 100\,\mathrm{s}$.

N	smooth solution		discontinuous solution	
	$\varepsilon_N^{\Delta z}(t)$	$\Upsilon_N(t)$	$\varepsilon_N^{\Delta z}(t)$	$\Upsilon_N(t)$
50	1.1384×10^{-1}	——	2.2207	——
100	6.0321×10^{-2}	0.9163	1.3541	0.7137
200	3.1950×10^{-2}	0.9168	7.4303×10^{-1}	0.8658
400	1.6291×10^{-2}	0.9717	4.5034×10^{-1}	0.7224
800	7.7365×10^{-3}	1.0743	2.9061×10^{-1}	0.6319
1600	3.8611×10^{-3}	1.0027	1.5534×10^{-1}	0.9037

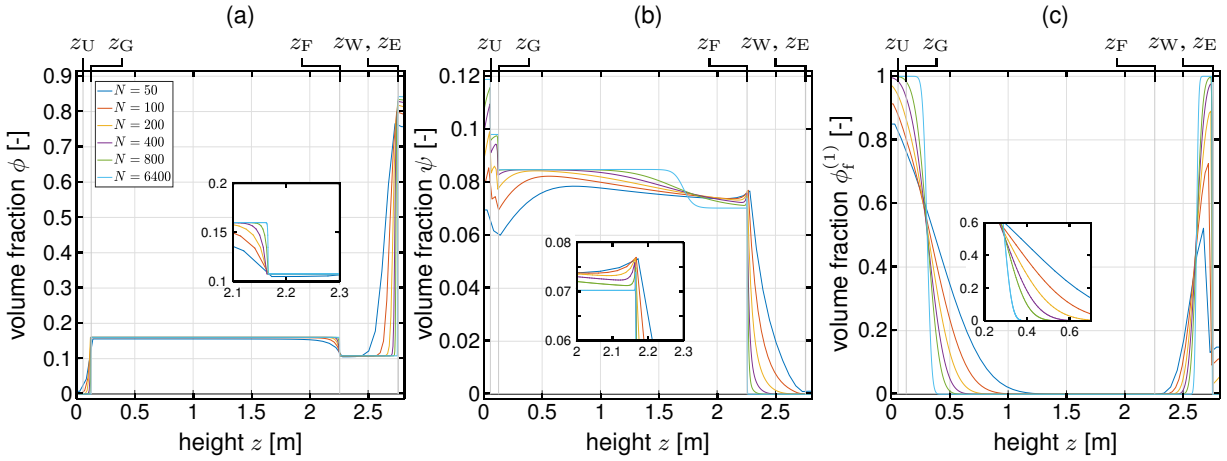

FIGURE 10. Example 2 (accuracy test, discontinuous solution): Volume fraction of aggregates ϕ, solids ψ and initial water $\phi_{\mathrm{f}}^{(1)}$ at $T = 100\,\mathrm{s}$ for various values of N.

5.3. **Examples 1 and 2: accuracy tests.** In Example 1, we assess the spatial convergence of the method by computing the error $\varepsilon_N^{\Delta z}(T)$ of a smooth solution. In this simulation, we set $q_{\mathrm{U}} = q_{\mathrm{G}} = q_{\mathrm{F}} = q_{\mathrm{W}} = q_{\mathrm{E}} = 0\,\mathrm{cm/s}$, use sinusoidal initial conditions for the volume fraction of aggregates ϕ and solids ψ and compute the numerical solution at a short time $T = 4\,\mathrm{s}$ before a discontinuity appears. Figure 9 shows the evolution of the numerical profiles of ϕ and ψ at $T = 4\,\mathrm{s}$ as the mesh is refined. In the left block of Table 2, the total estimated relative L^1 errors $\varepsilon_N^{\Delta z}(T)$ and the corresponding estimated orders of convergence $\Upsilon_N(T)$ are presented. As expected for a first-order method applied to smooth data, the convergence rate approaches one.

In Example 2, we start from a column filled with fluid at $t = 0\,\mathrm{s}$, when we start pumping aggregates, solids, fluid, and wash water, with flow rates $(q_{\mathrm{U}}, q_{\mathrm{F}}, q_{\mathrm{G}}, q_{\mathrm{W}}) = (2.0217, 2.0, 0.9605, 0.2)\,\mathrm{cm/s}$ and $\phi_{\mathrm{G}} = 1$, $\phi_{\mathrm{F}} = \phi_{\mathrm{W}} = 0$, $\psi_{\mathrm{F}} = 0.1$ and $\psi_{\mathrm{G}} = \psi_{\mathrm{W}} = 0$. In Figure 10, we can see the numerical discontinuous solutions of ϕ, ψ and $\phi_{\mathrm{f}}^{(1)}$ at $T = 100\,\mathrm{s}$ for different values of N. The right block of Table 2 displays the total approximate relative L^1 errors $\varepsilon_N^{\Delta z}(T)$ and the corresponding convergence rates $\Upsilon_N(T)$. As expected, in the presence of discontinuities, the observed orders are slightly below those obtained for smooth solutions.

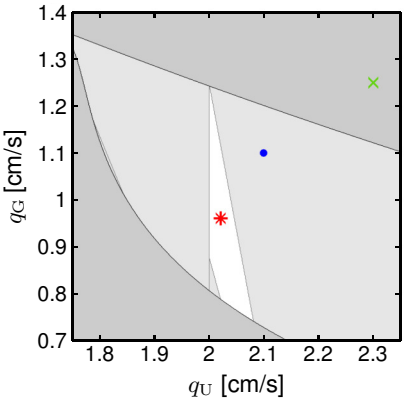

FIGURE 11. Examples 3 to 7: operating chart with $(q_F, q_W) = (2.0, 0.2)$ cm/s. The red point $(q_U, q_G) = (2.0217, 0.9605)$ cm/s lies in the white region where a desired steady state is feasible, whereas the blue and green points $(2.1, 1.1)$ cm/s and $(2.3, 1.25)$ cm/s, respectively, lie in the grey region, where some conditions but not all are satisfied and a desired steady state will not be attained.

5.4. **Examples 3 and 4: achieving a desired steady state of liquid and solid phases.** In Examples 3 and 4, we start from a column filled only with fluid at time $t = 0$ s, when we start pumping aggregates, solids, fluid, and wash water, with $\phi_G = 1$ and $\phi_F = \phi_W = 0$, $\psi_F = 0.1$ and $\psi_G = \psi_W = 0$. The flow rates corresponding to the red point marked in the operating chart of Figure 11: $(q_U, q_F, q_G, q_W) = (2.0217, 2.0, 0.9605, 0.2)$ cm/s. In Example 3, we simulate until $t = 300$ s, and in Example 4, until $t = 3000$ s.

For Example 3, Figures 12(a) and (b) show that the numerical solution evolves into a steady state where the aggregates have a low froth concentration in zone 2, the collection zone, a slightly lower one in most of zone 3, and a thin froth layer forming at the top of the column within zone 3 below the wash water inlet. Initially, most of the solids settle downwards from the inlet but some of them rise and reach zone 3 due to the lack of bubbles in that zone initially. When aggregates reach zone 3, the solids stop rising and settle so that, after about 100 s, a desired steady state is achieved for solids, since they remain below the feed level z_F.

The corresponding time evolution of the liquid components for $t = 300$ s is shown in Figures 12(c) to (f). The volume fraction of initial water $\phi_f^{(1)}$ decreases significantly throughout the process. The initial body of water is displaced mainly by the feed water $\phi_f^{(3)}$ and the wash water $\phi_f^{(4)}$. The feed water reaches the part of the column above z_F and replaces the initial water. In the upper part of the column, near the effluent, wash water appears and slowly increases until it reaches $\phi_f^{(4)} = 1$, so wash water completely displaces the other components in zone 4. After $t = 100$ s, the wash water slowly moves downwards through zone 4, which indicates positive bias flow in zone 4.

In Example 4 we have repeated this simulation for a longer time, $t = 3000$ s, see Figure 13 in order to see when the liquid components reach a steady state and which configuration the steady state achieves. As seen in Figure 13(c), after approximately 2500 s, the initial water leaves the column completely through the underflow, as one would expect. The other components reach a steady state around this time. The slimes and the feed water descend and remain in the part of the column below the feed inlet, leaving also through the underflow, whereas the wash water slowly fills zone 4 and, after $t = 2000$ s, a small part of its volume fraction travels down the column and leaves through the underflow. This positive bias flow is necessary to effectively wash the entrained

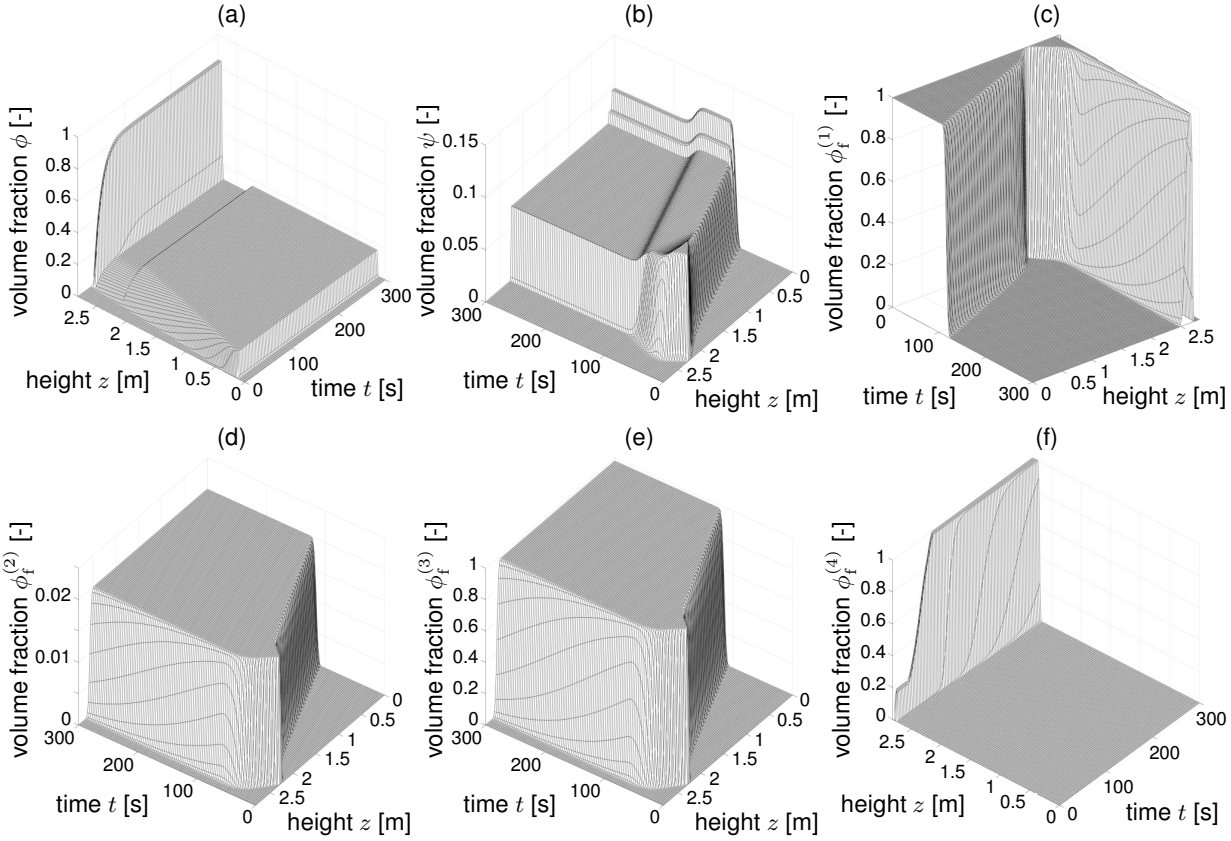

FIGURE 12. Example 3 (achieving a desired steady state, short-time simulation): simulation from $t = 0\,\mathrm{s}$ to $300\,\mathrm{s}$, with $N = 1600$, of the volume fractions of (a) aggregates ϕ, (b) solids ψ, (c) the initial water $\phi_{\mathrm{f}}^{(1)}$, (d) the slimes $\phi_{\mathrm{f}}^{(2)}$, (e) the feed water $\phi_{\mathrm{f}}^{(3)}$, and (f) the wash water $\phi_{\mathrm{f}}^{(4)}$.

particles in the liquid part below z_{F}, in zone 3, so that they do not move up to zone 4 and report into the effluent. Hence, the effluent volume fractions are approximately $\phi \approx 0.8$, $\psi = 0$, and $\phi_{\mathrm{f}} \approx 0.2$, and that the effluent liquid entirely comes from the wash water. This is an ideal scenario where no feed water leaves through the effluent, and moreover, aggregates are washed of entrained solid particles in zone 3 by the wash water that moves down the column. Figure 13 illustrated that the water component dynamics detailed before do not affect the steady state reached for ϕ and ψ before $t = 300\,\mathrm{s}$ (shown in Figure 12).

5.5. **Example 5 (gas-free configuration).** Figure 12(b) of Example 3 (or equivalently, Figure 13(b) of Example 4) shows that transitorily solid particles are entrained into zone 3. To illustrate that this phenomenon is related to the injection of gas, we performed an additional simulation using the same parameters as above but setting both the initial bubble volume fraction and the volumetric flow of gas to zero, i.e., we use $\phi_{\mathrm{G}} = \phi_{\mathrm{F}} = \phi_{\mathrm{W}} = 0$, $\psi_{\mathrm{F}} = 0.1$ and $\psi_{\mathrm{G}} = \psi_{\mathrm{W}} = 0$, and $(q_{\mathrm{U}}, q_{\mathrm{F}}, q_{\mathrm{G}}, q_{\mathrm{W}}) = (2.021, 2.0, 0, 0.2)\,\mathrm{cm/s}$. In this gas-free configuration, shown in Figure 14, we observe a significant change in the behavior of the solids. In contrast to Example 3, the solids do not reach zone 3 and remain below z_{F}. In Figures 14(b) to (e) we show the water components

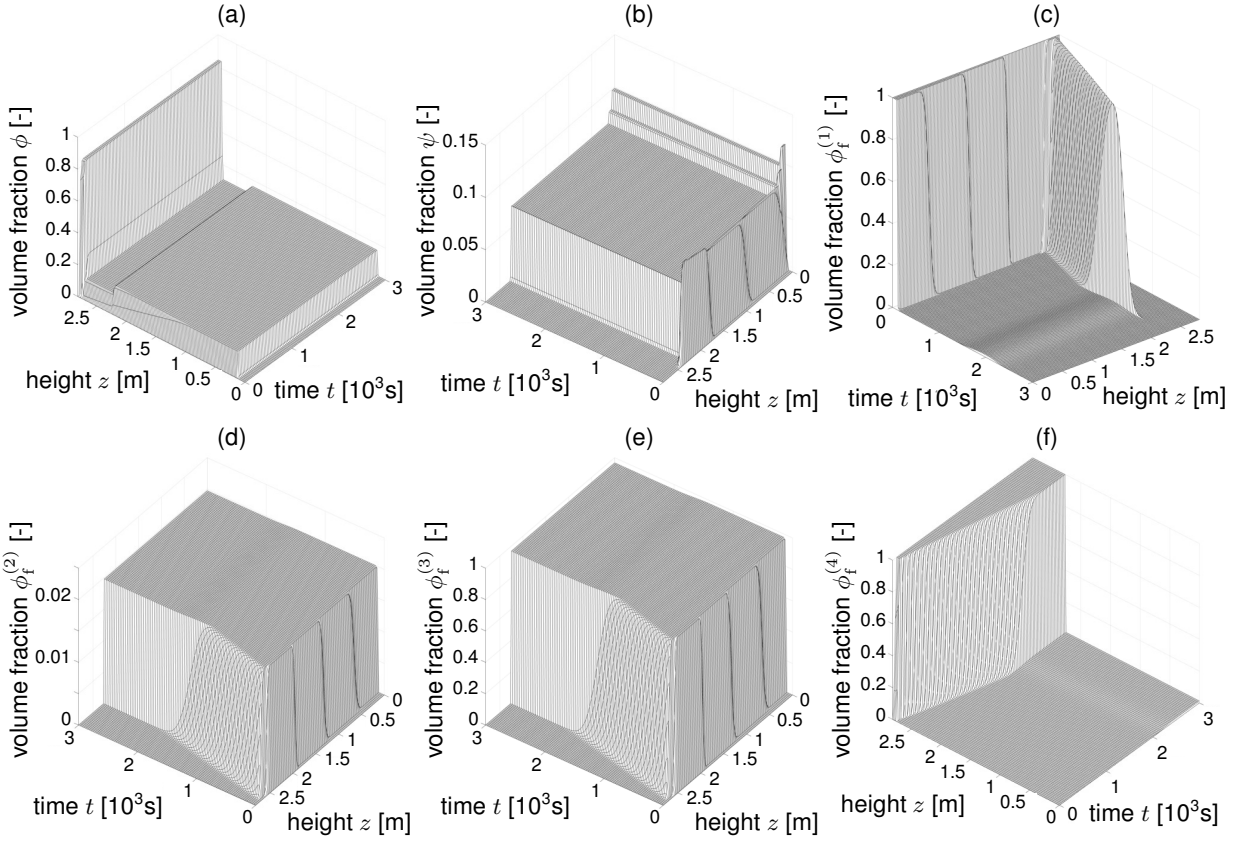

FIGURE 13. Example 4 (achieving a desired steady state, long-time simulation): simulation from $t = 0\,\text{s}$ to $3000\,\text{s}$, with $N = 1600$, of the volume fractions of (a) aggregates ϕ, (b) solids ψ, (c) the initial water $\phi_f^{(1)}$, (d) the slimes $\phi_f^{(2)}$, (e) the feed water $\phi_f^{(3)}$, and (f) the wash water $\phi_f^{(4)}$.

dynamics for this case. As can be seen, the initial water eventually disappears after $t = 2500\,\text{s}$, approximately. It is also interesting to note that, once the initial water is out of the column, the wash water travels down the column, and a small quantity leaves through the underflow. The behavior of the water components in this case is very similar to the case with gas.

5.6. **Example 6 (dynamic transition between steady states).** We now analyze the dynamic transition between three steady states obtained using the three different points in the operating chart in Figure 11, exploring the effects of modifying the flow rates q_U and q_G on the evolution of aggregates and solids. Initially, we use the flow rates $(q_U, q_F, q_G, q_W) = (2.0217, 2.0, 0.9605, 0.2)\,\text{cm/s}$, which are represented by the red star in Figure 11, and simulate until $t = 500\,\text{s}$ where the system reaches a desired steady state for aggregates and solids, as Figure 15 shows. As we have seen in Examples 3 and 4, at $t = 500\,\text{s}$ the liquid components have not reached a steady state yet; see Figures 13(c) to (f). Once the first steady state is reached, we change the underflow and gas flow rates to $(q_U, q_G) = (2.1, 1.1)\,\text{cm/s}$. These values correspond to the blue point in Figure 11. After this change, the dynamics of the vessel change: bubbles flow downwards and eventually leave through the bottom of the column, resulting in an undesired steady state reached at approximately

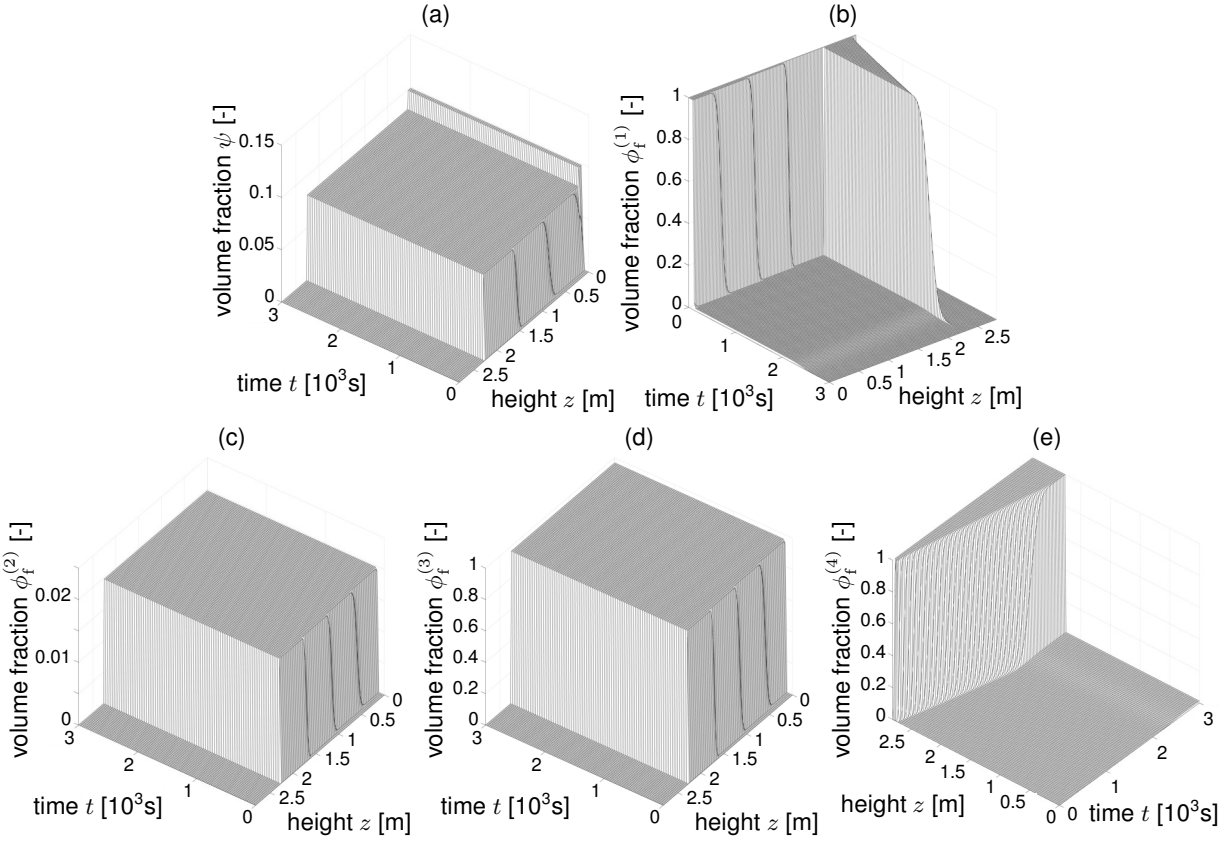

FIGURE 14. Example 5 (gas-free configuration): simulation from $t = 0\,\mathrm{s}$ to $3000\,\mathrm{s}$, with $N = 1600$, of the volume fractions of (a) solids ψ, (b) the initial water $\phi_{\mathrm{f}}^{(1)}$, (c) the slimes $\phi_{\mathrm{f}}^{(2)}$, (d) the feed water $\phi_{\mathrm{f}}^{(3)}$, and (e) the wash water $\phi_{\mathrm{f}}^{(4)}$.

$t = 2500\,\mathrm{s}$. At this time, we readjust the flow rates again to the values $(q_{\mathrm{U}}, q_{\mathrm{G}}) = (2.3, 1.25)\,\mathrm{cm/s}$ represented by the green cross and located in the dark gray region of the operating chart in Figure 11. Now aggregates remain in an undesired steady state, leaving through the bottom of the column but with a slightly different volume fraction. Despite these dynamic transitions, it can be observed in Figure 15 that the solids always remain below the feed entry level z_{F} throughout the simulation, except for a small time at the beginning. Figures 15(c) to (f) show the dynamics of the liquid components during this simulation. As mentioned, these components do not reach steady state with the first pair of flow rates $(q_{\mathrm{U}}, q_{\mathrm{G}})$ chosen, but they do for the subsequent two.

5.7. **Example 7 (recovery of a desired steady state).** We continue the simulation of Example 6 by adjusting the flow rates back to the red point in the white zone of the operating chart in Figure 11 to see if we can obtain a desired steady state, i.e, if we can reach a steady state with no aggregates leaving through the underflow and no solids above the feed inlet. As Figure 16 shows, at $t = 7500\,\mathrm{s}$, a desired steady state is reached, the same we saw at $t = 500\,\mathrm{s}$ in Figure 12. In Figure 16(c) to (f), we can see the steady states that the liquid components settle into.

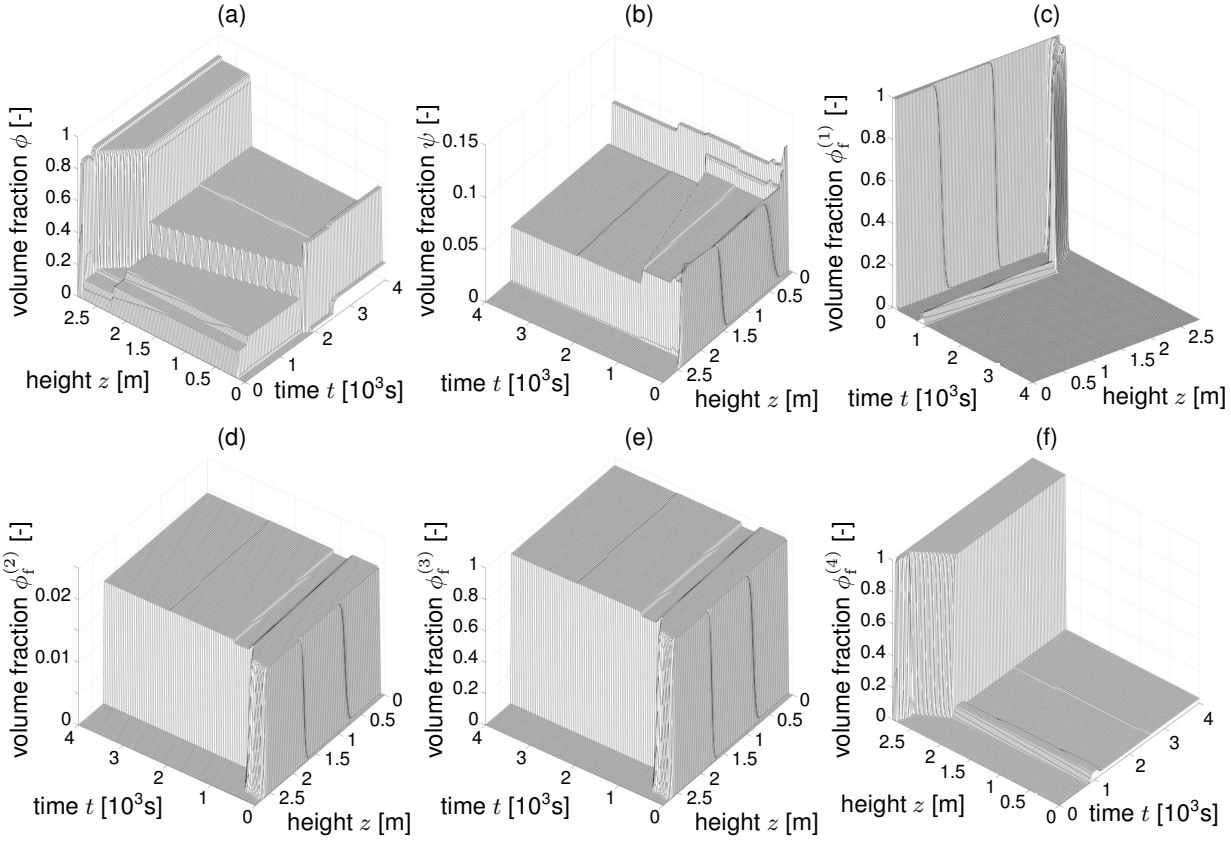

FIGURE 15. Example 6 (dynamic transition between steady states): simulation from $t = 0\,\mathrm{s}$ to $4000\,\mathrm{s}$, with $N = 1600$, of the volume fractions of (a) aggregates ϕ, (b) solids ψ, (c) the initial water $\phi_{\mathrm{f}}^{(1)}$, (d) the slimes $\phi_{\mathrm{f}}^{(2)}$, (e) the feed water $\phi_{\mathrm{f}}^{(3)}$, and (f) the wash water $\phi_{\mathrm{f}}^{(4)}$.

6. Conclusions and future work

The present work extends the two-phase flotation model proposed by the authors in [10] to a three-phase model, given by a convection-diffusion-reaction system, that includes the fluid dynamics, in particular, the transport of several liquid components are included. A new partial differential equation is introduced to model the dynamics of all the different elements that constitute the fluid of the column. The evolution of each component is described by a percentage vector. For the numerical simulation examples, we divide the fluid into four components: the water that initially fills the flotation column, fine solid particles transported with the fluid, called slimes, feed water and wash water, which are the most relevant in the context of the flotation process, but more components can be considered.

The governing model is described in detail, including the constitutive functions modelling the settling of the hydrophilic solid particles, the rising of the aggregates through the column and the diffusive term that describes the drainage of the liquid between bubbles when they accumulate at the top of the column forming a foam layer. All volume fractions are discontinuously space due

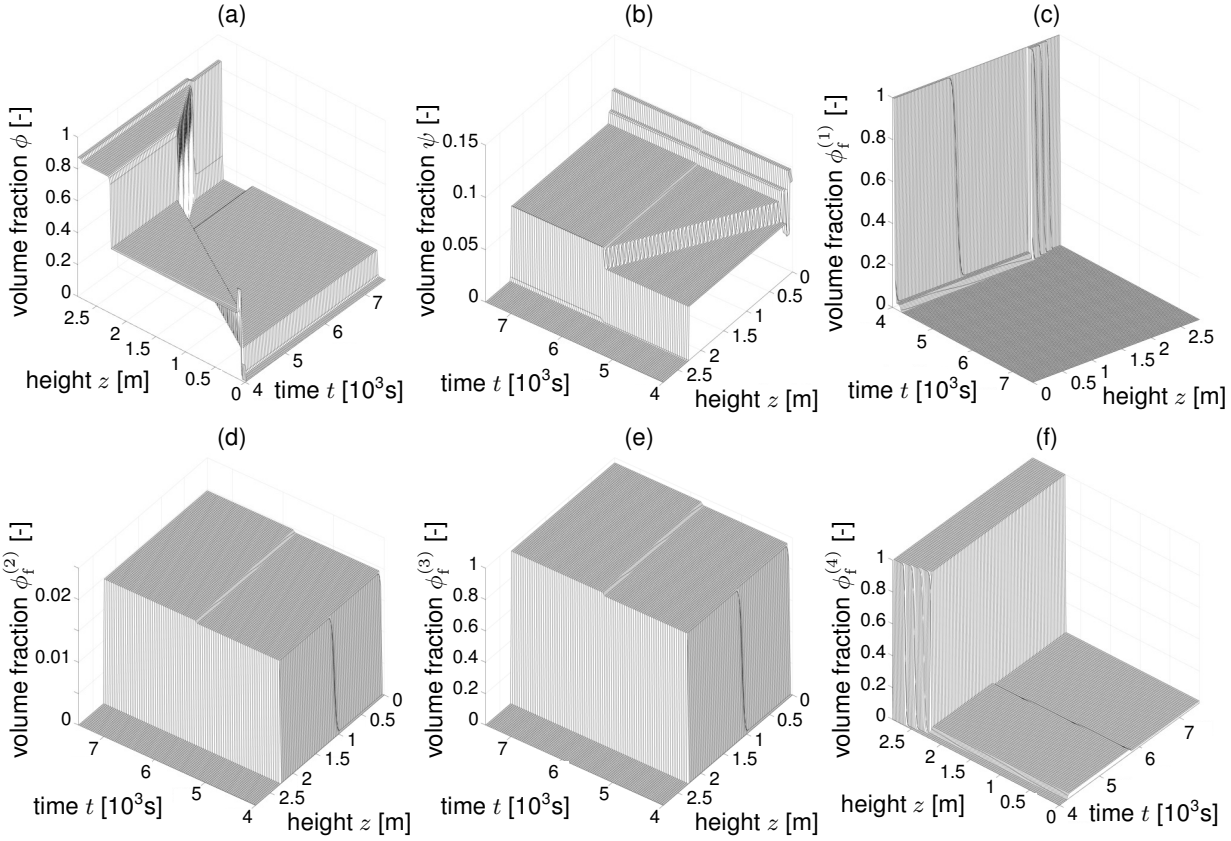

FIGURE 16. Example 7 (recovery of a desired steady state): simulation from $t = 4000\,\mathrm{s}$ to $7500\,\mathrm{s}$, with $N = 1600$, of the volume fractions of (a) aggregates ϕ, (b) solids ψ, (c) the initial water $\phi_{\mathrm{f}}^{(1)}$, (d) the slimes $\phi_{\mathrm{f}}^{(2)}$, (e) the feed water $\phi_{\mathrm{f}}^{(3)}$, and (f) the wash water $\phi_{\mathrm{f}}^{(4)}$.

to the presence of inlets and outlets of the column, and have spatial-temporal discontinuity curves due to the degenerate parabolic PDEs.

The study of the possible steady states with a froth layer at the top of the column and a positive bias flow (a small quantity of water travelling downwards from the wash water inlet), called desired steady states, performed in Section 4 showed that they are feasible if ten inequalities are satisfied. These inequalities can be represented in operating charts that show the values of $(q_{\mathrm{U}}, q_{\mathrm{G}})$.

The present treatment is based on a first-order accurate scheme. Future directions of work could therefore consist in improving formal order of accuracy while maintaining the IRP property through the application of high-order weighted essentially non-oscillatory (WENO) reconstructions including a scaling limiter, as was originally proposed in [34–36] (see [3]).

ACKNOWLEDGEMENTS

R.B. is supported by ANID (Chile) through Fondecyt project 1250676; Centro de Modelamiento Matemático (CMM), BASAL project FB210005; and CRHIAM, project ANID/FONDAP/1523A0001. M.C.M. is supported by grants PID2020-117211GB-I00 funded by MCIN/AEI/10.13039/501100011033,

PID2023-146836NB-I00 funded by MCIU/AEI/10.13039/501100011033 and project CIAICO/2021/227. Y.V. is supported by SNI-SENACYT (Panama) and CEMCIT-AIP.

References

[1] C. Acosta and S. Jerez, Convergence of entropy stable schemes for degenerate parabolic equations with a discontinuous convection term. *ESAIM: Math. Model. Numer. Anal.* **57** (2023) 1445–1472

[2] M. Ancellin, B. Després, and S. Jaouen, Extension of generic two-component VOF interface advection schemes to an arbitrary number of components. *J. Comput. Phys.* **473** (2023) article 111721.

[3] J. Barajas-Calonge, R. Bürger, P. Mulet and L.M. Villada, Invariant-region-preserving WENO schemes for one-dimensional multispecies kinematic flow models. *J. Comput. Phys.* **537** (2025), article 114081.

[4] A. Baumgart and G. Blanquart. Ensuring $\sum_s y_s = 1$ in transport of species mass fractions. *J. Comput. Phys.* **513** (2024) article 113199.

[5] F. Betancourt, R. Bürger, S. Diehl, L. Gutiérrez, M. C. Martí and Y. Vásquez, A model of froth flotation with drainage: Simulations and comparison with experiments. *Minerals* **13** (2023) article 344 (24pp).

[6] M. R. Bhole and J. B. Joshi, Modelling gas holdup in flotation column froths. *Canad. J. Chem. Eng.* **85** (2007) 369–373.

[7] R. Bürger, J. Careaga, S. Diehl and R. Pineda, A model of reactive settling of activated sludge: Comparison with experimental data. *Chem. Eng. Sci.* **267** (2023) article 118244 (13pp).

[8] R. Bürger, J. Careaga, S. Diehl and R. Pineda, Numerical schemes for a moving-boundary convection-diffusion-reaction model of sequencing batch reactors. *ESAIM: Math. Model. Numer. Anal.* **57** (2023) 2931–2976.

[9] R. Bürger, S. Diehl and M. C. Martí, A system of conservation laws with discontinuous flux modelling flotation with sedimentation. *IMA J. Appl. Math.* **84** (2019) 930–973.

[10] R. Bürger, S. Diehl, M. C. Martí and Y. Vásquez, A degenerating convection-diffusion system modelling froth flotation with drainage. *IMA J. Appl. Math.* **87** (2022) 1151–1190.

[11] R. Bürger, S. Diehl, M. C. Martí and Y. Vásquez, A difference scheme for a triangular system of conservation laws with discontinuous flux modeling three-phase flows. *Netw. Heterog. Media* **18** (2023) 140–190.

[12] J. E. Dickinson and K. P. Galvin, Fluidized bed desliming in fine particle flotation, Part I. *Chem. Eng. Sci.* **108** (2014) 283–298.

[13] S. Diehl, Continuous sedimentation of multi-component particles. *Math. Meth. Appl. Sci.* **20** (1997) 1345–1364.

[14] S. Diehl, Operating charts for continuous sedimentation I: control of steady states. *J. Eng. Math.* **41** (2001) 117–144.

[15] S. Diehl, Operating charts for continuous sedimentation II: step responses. *J. Eng. Math.* **53** (2005) 139–185.

[16] S. Diehl, Operating charts for continuous sedimentation III: control of step inputs. *J. Eng. Math.* **54** (2006) 225–259.

[17] S. Diehl, Operating charts for continuous sedimentation IV: limitation for control of dynamic behaviour. *J. Eng. Math.* **60** (2008) 249–264.

[18] S. Diehl, A regulator for continuous sedimentation in ideal clarifier-thickener units. *J. Eng. Math.* **60** (2008) 265–291.

[19] S. Diehl, A uniqueness condition for nonlinear convection-diffusion equations with discontinuous coefficients. *J. Hyperbolic Differential Equations* **6** (2009) 127–159.

[20] R. Droste and R. Gehr, Theory and Practice of Water and Wastewater Treatment, 2nd edn. Wiley, Hoboken, NJ, USA, 2019.

[21] M.J. Mankosa, J.N. Kohmuench, and G.H. Luttrell, Column flotation. Chapter 7.1 of R. C. Dunne, S. K. Kawatra and C. A. Young (Eds.), SME Mineral Processing & Extractive Metallurgy Handbook, Society for Mining, Metallurgy, and Exploration, Englewood, CO, USA, 2019, pp. 913–930.

[22] B. Engquist and S. Osher, One-sided difference approximations for nonlinear conservation laws. *Math. Comp.* **36** (1981) 321–351.

[23] J. A. Finch and G. S. Dobby, Column Flotation, Pergamon Press, London, UK, 1990.

[24] M.C. Fuerstenau and P. Somasundaran, Flotation. Chapter 8 in M.C. Fuerstenau and K.N. Han (eds.), Principles of Mineral Processing, Society for Mining, Metallurgy, and Exploration, Englewood, CO, USA, 2019, pp. 245–306.

[25] P. M. Ireland and G. J. Jameson, Liquid transport in a multi-layer froth. *J. Colloid Interface Sci.* **314** (2007) 207–213.

[26] Z. Huang and E. Johnsen, A consistent and conservative phase-field method for compressible N-phase flows: Consistent limiter and multiphase reduction-consistent formulation. *J. Comput. Phys.* **501** (2024) article 112801.

[27] S. Jaouen and F. Lagoutière, Numerical transport of an arbitrary number of components. *Comput. Meth. Appl. Mech. Engrg.* **196** (2007) 3127–3140.
[28] D. Kuzmin and H. Hajduk, Property-preserving numerical schemes for conservation laws, World Scientific, 2024.
[29] L. Metcalf and H.P. Eddy, Wastewater Engineering. Treatment and Resource Recovery, 5th edition. McGraw-Hill, New York, USA (2014).
[30] R. Pal and J. H. Masliyah, Flow characterization of a flotation column. *Canad. J. Chem. Eng.* **67** (1989) 916–923.
[31] P. Quintanilla, S. J. Neethling and P. R. Brito-Parada, Modelling for froth flotation control: A review. *Minerals Eng.* **162** (2021), article 106718.
[32] J. F. Richardson and W. N. Zaki, Sedimentation and fluidisation: Part I. *Trans. Inst. Chem. Engrs. (London)* **32** (1954) 35–53.
[33] J. Vandenberghe, J. Chung, Z. Xu and J. Masliyah, Drift flux modelling for a two-phase system in a flotation column. *Canad. J. Chem. Eng.* **83** (2005) 169–176.
[34] X. Zhang and C.-W. Shu, On maximum-principle-satisfying high order schemes for scalar conservation laws. *J. Comput. Phys.* **229** (2010) 3091–3120.
[35] X. Zhang and C.-W. Shu, On positivity-preserving high order discontinuous Galerkin schemes for compressible Euler equations on rectangular meshes. *J. Comput. Phys.* **229** (2010) 8918–8934.
[36] X. Zhang and C.-W. Shu, Maximum-principle-satisfying and positivity-preserving high-order schemes for conservation laws: survey and new developments. *Proc. Roy. Soc. A* **467** (2134) (2011) 2752–2776.

Centro de Investigación en Ingeniería Matemática (CI^{2}MA)

PRE-PUBLICACIONES 2025

2025-06 Jessika Camaño, Ricardo Oyarzúa, Katherine Rojo: *A momentum and mass conservative pseudostress-based mixed finite element method for the Stokes problem*

2025-07 Aníbal Coronel, Fernando Huancas, Mauricio Sepúlveda: *Theoretical and numerical approaches of reaction term identification in a SIS reaction diffusion system*

2025-08 Isaac Bermudez, Gabriel N. Gatica, Juan P. Silva: *A new Banach spaces-based mixed finite element method for the coupled Navier-Stokes and Darcy equations*

2025-09 Sergio Caucao, Gabriel N. Gatica, Saulo Medrado, Yuri D. Sobral: *A posteriori error analysis of mixed finite element methods for a regularized mu(I)-rheology model of granular materials*

2025-10 Veronica Anaya, Gerardo Chowell, Felipe Jara, Mauricio Sepúlveda: *Optimal control of inter-population disease spread via reaction–diffusion models*

2025-11 Ramiro Acevedo, Rommel Bustinza, Christian Gómez: *A transient Eddy current problem via potential formulation with current excitation*

2025-12 Abraham J. Arenas, Juan Barajas-Calonge, Gilberto González-Parra, Luis M. Villada: *A second-order nonstandard finite difference scheme for eco-epidemiological predator-prey models*

2025-13 Alonso J. Bustos, Sergio Caucao, Gabriel N. Gatica: *Mixed-primal and fully-mixed formulations for the convection-diffusion-reaction system based upon Brinkman–Forchheimer equations*

2025-14 Gabriel N. Gatica, Zeinab Gharibi, Ricardo Oyarzúa: *Banach spaces-based fully mixed finite element methods for the n-dimensional Boussinesq problem with temperature-dependent parameters*

2025-15 Sergio Caucao, Ricardo Oyarzúa, Segundo Villa-Fuentes: *A priori and a posteriori error analyses of a fully-mixed finite element method for the coupled Navier Stokes / Darcy problem*

2025-16 Juan Barajas-Calonge, Raimund Bürger, Pep Mulet, Luis M. Villada: *A second-order invariant-region-preserving scheme for a transport-flow model of polydisperse sedimentation*

2025-17 Raimund Bürger, Stefan Diehl, María Carmen Martí, Yolanda Vásquez: *A numerical scheme for a model of a flotation column including the transport of liquid components*

Para obtener copias de las Pre-Publicaciones, escribir o llamar a: Director, Centro de Investigación en Ingeniería Matemática, Universidad de Concepción, Casilla 160-C, Concepción, Chile, Tel.: 41-2661324, o bien, visitar la página web del centro: `http://www.ci2ma.udec.cl`







Centro de Investigación en
Ingeniería Matemática (CI²MA)
Universidad de Concepción

Casilla 160-C, Concepción, Chile
Tel.: 56-41-2661324/2661554/2661316
http://www.ci2ma.udec.cl